Crack Identification at the Welding Joint with a Smart Coating Sensor

By
Xin Wang

A Thesis Submitted to the Faculty of Graduate Studies of

The University of Manitoba

In partial fulfilment of the requirements of the degree of

MASTER OF SCIENCE

Department of Mechanical Engineering

University of Manitoba

Winnipeg, Manitoba

ABSTRACT

In order to avoid the money loss and injuries caused by the structural damage, early detection of the small cracks in a structure is very important. Conventional damage detection techniques, such as ultrasonic methods, strain energy methods, magnetic field methods, etc., are usually lack of sensitivity or hard to be applied to different surfaces requiring complex sensing systems. In this thesis, a new piezoelectric coating sensor is developed to detect the crack initiation, and it can apply to any surfaces of interest. Two sensitive crack measurement methods, wavelet Entropy and Frequency Comparison Function (FCF), are introduced to evaluate the crack for the structure based on the vibration signals from the new sensor. During operating, the piezoelectric composite coating sensor is applied at the welding joint of a vibrating structure to send warning and dynamic signals for damage detection and evaluation, when the crack occurs. Entropy and FCF methods are introduced to quantify the weak dynamic perturbations, which are caused by the strain concentration and/or crack breathing at the crack tip. A finite element model (FEM) of a welded beam subjected to the dynamic base motions is established for case studies to show the efficiency of the proposed smart coating and measurement methods. The effects of strain/stress concentration and crack breathing on the structural dynamic response are simulated by creating the nonlinear material property around the crack area and the contact pair of the crack walls, respectively. From simulations, both methods are found to be sensitive to the initiated closed crack. The Entropy method can detect a crack of 5% thickness of the beam thickness. Meanwhile, it is feasible and sensitive for both open and closed cracks detection. The FCF method can detect a closed crack with a size of 3% of the beam thickness. In addition, FCF is fast and efficient with no required data pre-progressing, like the filtering and smoothing functions, and can hence be used for real-

time crack detection. Experimental validations are conducted for both methods, and the results prove high sensitivity and feasibility of both proposed crack detection methods.

ACKNOWLEDGMENTS

I would like to express my deepest gratitude to my advisor, Dr. Nan Wu for his full support, expert guidance, encouragement and assistance throughout this work. I sincerely appreciate for his valuable time, patience, counsel and insight to carry this thesis. This thesis would not have been possible without his guidance and support. I also want to thank my committee members, Prof. Carl Ho and Prof. Guozhen Zhu, for their constructional comments and guidance.

I would also like to thank the colleagues in our lab and my friends for the great time we shared during master study, my sincere gratitude also expressed to the professors who provided me with kind-hearted help in the last 2 years.

Last but not the least I want to thank three most important people in my life, my parents and my grandpa, for their unconditional support and endless love all along, it is not possible for me to achieve my goals without their inspiration.

TABLE OF CONTENT

LIST OF TABLES

LIST OF FIGURES

LIST OF SYMBOLS

AE	Acoustic Emission
WT	Wavelet Transform
SampEn	Sample Entropy
ApEn	Approximate Entropy
MSE	Multi-Scale Entropy
PE	Permutation Entropy
MPE	Multiscale Permutation Entropy
FCF	Frequency Comparison Function
FRF	Frequency Response Function
FEM	Finite Element Model
FEA	Finite Element Analysis
HAZ	Heat Affected Zone
BM	Base Metal
WM	Weld Metal
FZ	Fusion Zone
e_{31}	Piezoelectric coupling coefficients for Stress-Charge form
d_{31}	Piezoelectric coupling coefficients for Strain-Charge form
C_v	Electrical capacity of the piezoelectric materials
L	Length of the beam
l_p	Length of the piezoelectric patch
W	Width of the beam
w_p	Width of the piezoelectric patch

H	Thickness of the beam
h_p	Thickness of the piezoelectric patch

LIST OF COPYRIGHTED MATERIALS

Materials used in the section 3 of this thesis are reproduced, with modifications from Wang X and Wu N, 2019, “Crack identification at welding joint with a new smart coating sensor and entropy”, *Mechanical Systems and Signal Processing*, **124**, 65-82.

Upon transfer of the copyright to the Elsevier publishing, the right to include the final published version of the mentioned records were granted back to the authors for the purpose of inclusion in the thesis.

1. INTRODUCTION

1.1. Motivation of this Research

Since initial damages in a structure, such as cracks, notches, and delamination, can lead to calamitous and irreparable failure, early identification of these structural damages has been a common topic among researchers during the recent decades. There are varieties of common techniques in use for damage detection, like ultrasonic methods [1], acoustic applications [2, 3], thermal field techniques [4] and magnetic field methods [5]. All these methods are either visual or experimental applications, and different shortcomings happen when applying these techniques, including long inspection time, high cost, sensitive to material and environment interferes, unable to reach damaged area and unable to realize continuous real-time detection of damages.

In recent decades, new non-destructive damage detection techniques have been developed [6]. Acoustic emission (AE), as a widely used tool, allows damage estimation despite the appearance and condition of the objects and can detect defects at their initiation. However, the noise has always been a potential barrier since AE is quite sensitive to the nature of the material and the environmental interferes [7，8]. Vibration-based structural damage detection methods are also of great interest due to their online real-time continuous damage detection capabilities. It can be widely applied to any structural part and is quite cost-effective during long runs [9-12]. Besides, the smart materials can be employed in damage identification. Islam and Craig [13] developed a method for damage detection in composite structures by embedded piezoelectric sensors and actuators. Extensive researches on damage identification using piezoelectric materials have also been investigated [14-17]. It was proven that the identification sensitivity was enhanced by using smart materials. An efficient piezoelectric composite coating sensor combined with a separate piezoelectric harvester was also developed [18] to realize the on-board wireless fracture detection. Although it was possible to make a self-powered on-board damage detection sensor, estimation of the damage severity increment and the potential of the damage propagation cannot be realized by the sensor proposed in [18]. And an additional piezoelectric energy harvester has to be added to the design. Optimized sensor design with a self-powering ability and effective damage identification methodologies (both detection and estimation of damage severity increment) are desired.

1.2. Literature Review

In this section, the evolvement of the damage detection methods from conventional damage identification schemes to advanced vibration-based damage detection techniques is elaborated.

For an extended period, visual inspection is the basic and most common detection technique. However, this traditional method can only be applied for simple structures [19]. Conventional non-destructive tests, such as guided ultrasonic waves, optical fiber sensors, X-ray test, magnetic particle test, etc., have been well studied in the past decades [20]. Limitations are also evident that these techniques are time and money consuming. Some of these techniques are unable to reach the damaged area, and the on-line real-time continuous damage detection is hard to be realized. Hence, the vibration-based damage identification technique is developed to overcome these problems.

1.2.1. Previous studies on vibration-based damage detection technologies

Vibration signals of a structure carry useful information about its healthiness. Numerous reviews have been published on vibration-based damage detection methodologies in the past several decades. It is known that the modal parameters (frequencies, mode shapes, and damping constant) are functions of the physical properties of a structure. Conversely, physical properties changes will cause detectable changes in the modal properties. By evaluating the vibration signals variation between the healthy structure and the damaged one, people can detect and even evaluate the physical damage. The dynamic characteristics lying in the vibration signals can be captured using the time history method [21, 22] as well as the methods based on the structural mode shape and its derivatives [23-25], frequencies [26], strain energy [27], modal damping ratio [28] and frequency response function [29, 30].

Generally, the excitation and response are measured and recorded in time domain during vibration test, and it is usually difficult to realize damage identification according to the time domain vibration data. Traditional signal processing method for structural testing and damage detection is to transfer time domain signals to the frequency domain, and the modal domain data can be further extracted from the frequency domain data. The conditions of the structure then can be discussed based on these frequency or modal domain data.

- Frequency response method

Cawley and Adams [26] conducted their damage detection research based on the study of the natural frequency. The frequency changes in a structure are measured with the use of the sensors. Sensors should be uniformly placed throughout the structure to detect the decrease or increase in natural frequencies induced by the stiffness change. So multiple sensors need to be applied, and this is a major disadvantage [31].

Huang et al. [32] developed a method, in which the frequency response is obtained from the second-order differential equation of motion. And the damage in a structure can be measured effectively once the frequency change reaches 5%. But it is difficult to excite a high natural frequency due to the higher energy needed. Meanwhile, the exact natural frequency is hard to get due to structural resonance.

In 2008, da Silva S et al. [33] introduced a fuzzy clustering algorithm to the FRF data processing to compress the data. In order to realize damage detection effectively, the original FRF data should be used. However, the amount of the data to be processed is too large that compression should be pre-processed without information loss.

Hwang and Kim [34] reported certain drawbacks in the FRF damage detection method, which is the inevitable noise interference. Even though the damaged frequency can be measured when the noise level is up to a range of 0 to 10%, the chance of error should be controlled under 2%. Hence, the noise level should be kept under 5% for the accuracy requirement. Askegaard V and Mossing P [35] also proposed that the influence of environmental interferes such as temperature and humidity can be minimized by collecting the frequency readings for the damaged and healthy structures at the same time.

Yu et al. [36] developed an optimized damage detection method (including data selection, data normalization, projection, damage feature extraction, and fuzzy clustering analysis). And they applied it to a 6-bay truss bridge. The effects of environment distortions can be reduced with this optimized method. Moreover, this technique is sensitive to the structural damage changes but not sensitive to the environmental changes.

- Mode shape method

In the early 90s, Chen [37] developed the mode shape method to counter the drawbacks in the frequency response method. Pandey [25] proposed the use of mode shape curvature as the sensitive parameter for structural damage. Li et al. [38] and Wang and Qiao [39] employed mode shapes and frequencies to determine the sensitivity of the structural stiffness variation, and the changes in the higher-order mode shape derivatives were far more precise considering damage identification than the mode shapes. However, the higher-order derivatives show discontinuities at damage locations because they are more sensitive to the loss of stiffness and curvature of undamaged mode shape [22]. And the higher-order derivatives are hard to excite at ambient conditions. Doebling [9] and Fan and Qiao [40] proposed an idea that the smoothness of mode shape and mode shape curvature can be a quite effective parameter to realize the damage detection.

It could be summarized that the mode shape method can be affected by environmental noise since the mode shapes themselves are quite environment sensitive. Furthermore, the number of sensors required for damage detection and their position has to be determined accurately [41] in order to obtain the accurate and smooth mode shapes.

- Strain energy method

In addition to the frequency response and modal based methods, Shi et al. [42] proposed an effective damage detection technique based on the modal strain energy change. This method is based only the mode shapes and elemental stiffness matrices, which effectively wipes out the external or environmental interferes. And it can locate damages in the area with low stiffness reduction of 10% [43]. Wang and Li [44] proposed a method based on the modal strain energy to identify damage which can be applied under lower natural frequencies. Strain energy method also possessed some disadvantages. It might indicate errors in case the data are limited, and the presence of noise can also affect the testing data as well.

In general, traditional frequency and modal analysis methods usually need complex sensing system, and most of them are too sensitive to environmental interference.

In order to overcome the complex sensor systems and their limitations in practical applications, Wu et al. [18] reported a low cost and efficient damage detection module. The major part of the module is a piezoelectric composite coating, and the sketch is shown in figure 1-1. This coating is composed of a piezoelectric layer, a conductive layer, and an insulator layer. It is easy to be applied on rough surfaces of engineering structures. The successful detection of the crack initiation on a beam structure was realized through experimental study. But separate piezoelectric patch must be applied here to realize self-powering. The crack increment evaluation cannot be realized in this work.

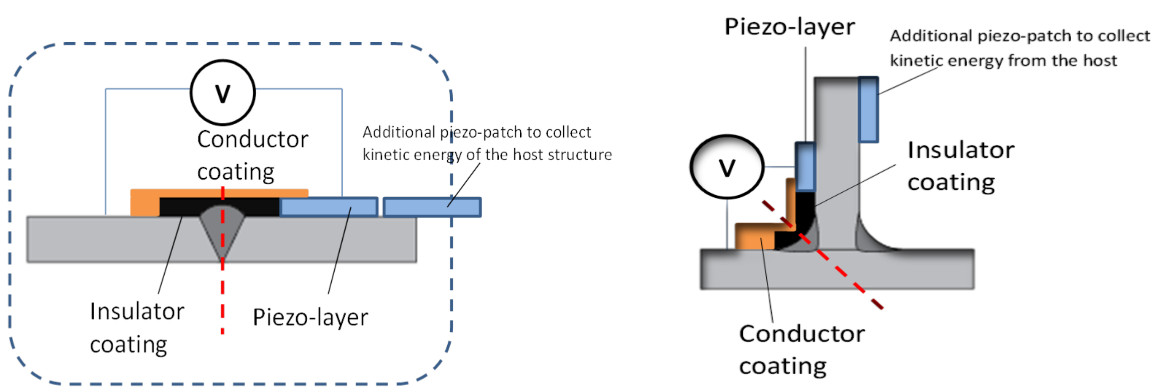

Figure 1-1. Damage detection module composed of piezoelectric composite coating with an additional energy harvesting piezo patch. [18]

1.2.2. Previous studies on Entropy

Most traditional vibration-based methods are based on direct changes in the modal parameters of the structure [45, 46]. Yan et al. [10] pointed out that modern vibration-based methods with new intelligent damage identification algorisms have more potential for damage detection than these traditional methods. New space and time-domain analysis techniques were developed to be popular signal processing methods for damage detection [47-49]. Recently, Wimarshana et al. [25, 26] presented a sensitive vibration-based damage detection method. It directly works on the time domain dynamic response processing. Wavelet transformation (WT) together with sample entropy (SampEn) are introduced as the efficient damage measurement agent for crack detection.

Entropy is defined as the loss of information in a time series or signal. In the past 2 to 3 decades, applications of the entropy methods to define periodicity or regularity in data analysis have been more and more popular. In this section, researches related to Entropy methods are discussed, and the pros and cons of these methods are analyzed.

The original entropy concept relies on the principle ones in Physics and Mathematics. In 1877, Ludwig Bolzman [52] proposed a visualized definition of the entropy. And it is the proportion to the logarithm of the number of microstates such an ensemble of ideal gas could occupy. In 1948, Claude Shannon [53] developed information entropy. The entropy formula here expresses the expected information content or uncertainty of a probability distribution. Let E_i stand for an event and p_i for the probability of event E_i to occur. Let there be n events E_1, …, E_n with probabilities p_1, …, p_n adding up to 1. Since the occurrence of events with smaller probability yields more information, a measure of information h should be a decreasing function of p_i. Shannon proposed a logarithmic function to express information $\mathrm{h}(p_i)$:

$$\mathrm{h}(p_i) = log_2\left(\frac{1}{p_i}\right), \tag{1-1}$$

which decreases from infinity to 0 for p_i ranging from 0 to 1. It reveals that the lower possibility of an event to occur, the larger the information amount of that message contains.

From the n number of information values $\mathrm{h}(p_i)$, the expected information content of a probability distribution, called entropy, is derived by weighing the information values $\mathrm{h}(p_i)$ by their respective probabilities:

$$\mathrm{H} = \sum_{i=1}^{n} p_i \, log_2\left(\frac{1}{p_i}\right), \tag{1-2}$$

where H stands for entropy in bits.

In the 50s, Kolmogorov and Sinai [54-56] employed entropy into dynamic signals and systems to evaluate their complexity for the first time. The entropy defined in these studies was called KS entropy, and it was concluded that KS entropy could be effectively applied to low-dimensional chaotic systems. However, it is not suitable to be applied to experimental data due to noise affection. In general, entropy increases with the increment of the complexity of dynamic response and has been already applied to many fields such as biomedicine [57, 58], human motion [59], image processing [60, 61] and financial market [62].

Apart from these applications as mentioned before, various entropy measures have been employed to detect damages for rotary machines. Pincus [63] developed approximate entropy (ApEn) to calculate the regularity in a time series, and it can classify complex systems concerning about 1000 data values. Dynamic complexity identification can then be realized by this method based on such a relatively small amount of data. The application of ApEn hence became so promising in a variety of contexts. An and Ou [64] proposed the mean curvature difference method based on ApEn and successfully located the damage in a shear frame structure. And even under tiny damages to the bearings, they can observe more than 200% increment in ApEn values. Multi-scale entropy (MSE) was proposed by Costa et al. [65, 66] to measure the entropy in physiological time series. H. Liu and M. Han [67] successfully introduced it into damage diagnosis for roller bearings. Similar bearing fault diagnosis has been conducted using permutation entropy (PE) [68] and multi-scale permutation entropy (MPE) [69] with improved accuracies. Moreover, Yang et al. [70] employed entropy measures for possible crack detection for beam structures, but the entropy itself was found to be not so sensitive to cracks. In order to solve this problem, Ren W X and Sun Z S [71] introduced the wavelet entropy to notch detection in beam structures based on Shannon entropy. The major advantage of wavelet transform (WT) is that it can amplify any desired segment of the signal to do the local analysis. However, this technique can only detect damage happening instantly. It is not practical in some applications while the period of crack happening is usually considerably short. The analysis result may also be interrupted by noise signals from the environments. Recently, Wimarshana et al. [50, 51] employed SampEn to detect breathing cracks in a vibrating beam structure. They realized the existing crack identification with high sensitivity and efficiency with both simulation and experimental studies. Here, sample entropy (SampEn), as a modification of ApEn, was proposed by Richman and Moorman [58] in 2000, it solves two major problems in entropy application: ignoring the noise effect and realizing measurement with limited available data. Combined with Wavelet transform (WT) and its optimization, Wimarshana et al. can detect cracks at its initial stage (8% of the beam thickness) [50]. However, they only considered the crack breathing effect of a closed crack. The effect of strain concentration/singularity at the crack tip was not studied and discussed to estimate the potential for the crack propagation. Meanwhile, the identification of an open crack through entropy was not realized.

1.2.3. Previous studies on Wavelet Transform (WT)

As a useful tool for signal processing to extract and amplify desired information from different kinds of data, the wavelet transform has been widely employed by researchers for damage detection [48, 72-76].

From the early 1990s, Newland [77] found out that wavelet transformation was feasible to provide more detailed information about non-stationary signals. He applied a wavelet analysis to the vibration signal of buildings caused by subway strains to detect the perturbation at the damaged area. Noori and Amand [78] also studied the characteristics of representative vibration signals under the wavelet transformation as an effective structure health monitoring technique. However, noise interfere is still a major limitation when applying WT to damage detection. Because the noises in vibration signals can also be amplified by WT and reduce the accuracy and effectiveness of damage detection using the classic time-frequency analysis. And those noises are inevitable, especially for some complex aeronautical structures. Identification and localization of the small cracks are also of great challenge for the time-frequency analysis with WT. Considering the problems in the time-frequency domain WT damage detection methods, Wang and Deng [79] proposed a damage detection method using spatial wavelet analysis. They detected the initiation of the crack by observing a sudden change in the spatial variation of the transformed deflection or displacement responses. Lam et al. [80] then provided a numerical simulation estimating the location and extent of a crack in a beam structure using the spatial wavelet transform. Based on the wavelet transformed displacement responses, the probability densities of different crack locations and extents were calculated.

However, as an auxiliary data processing tool, wavelet can be used to analyze time-domain vibration signals more efficiently with parameter tuning. Through a parameter tuning and optimization process, a WT can be used to amplify the desired damage induced perturbation signal without enlarging the noise signal in a different frequency range [49]. The advantage of WT is the ability to perform a local analysis of a signal by zooming on any desired segment of the temporal signal [71]. This fundamental feature of WT can be successfully merged with the entropy concept to reveal useful information concealed in signals.

1.3. Research objectives

Based on the literature review, the previous crack identification techniques always show a lack of early detection of the damage due to their lower sensitivities to initial small cracks. Most vibration-based methods need complex sensor systems, and the noises are inevitable. On the other hand, entropy, as a sensitive damage identification tool, is also limited for its long-running time. And its application to both open and closed cracks have not been studied yet. Meanwhile, with high uncertainty in the time domain, it is a great challenge to apply entropy method under random excitation, which is a more general working condition. In this thesis, research objectives considering these limitations are set as follows to develop an effective and sensitive onboard crack identification progress.

(1) Design a simple sensor for crack identification based on the sensor design of Wu et al. [18],
(2) Realize high-sensitive open crack identification with the new sensor design by introducing WT sample entropy measurement,

(3) Realize high-efficient real-time crack identification under arbitrary working load by introducing a derived frequency comparison function which is based on the frequency response function method.

These research objectives are realized in the following chapters by conducting simulation studies and experimental validations, and the achievements of these objectives are concluded in the final chapter, including some expectations on the future work.

1.4. Thesis organizations

The thesis is divided into five chapters: introduction, methodologies, followed by two results and discussion chapters covering the findings presented in 2 research papers, as well as a final chapter covering the conclusions and the future work.

2. SMART COATING SENSOR DESIGN AND DAMAGE IDENTIFICATION METHODOLOGIES

In this section, the design of the new smart coating sensor is explained in detail. Then, to analyze and estimate the crack severity increment with the dynamic signal from the smart coating sensor, two different methods, which are entropy measurement and Frequency Comparison Function (FCF), are introduced.

2.1. Smart Coating Sensor Design

Based on the design reported by Wu et al. [18], a new piezoelectric composite coating is developed to realize the crack identification at the welding joint area. Since the connection between the weldment and the base structure is quite delicate, the new smart coating will be applied on just the welding area, where fatigue damages usually happen.

The sensor design for the entropy measurement is shown in Figure 2-1 (a). The coating is composed of two piezoelectric patches/layers connected by a conductive layer and an insulator layer. It can act as a sensor to detect the severity of possible crack damage on rough surfaces of engineering structures, such as concrete and the welding joints. If the substructure is conductive, the piezoelectric patches/layers can be attached directly on the host structure through a conductive connection. The piezoelectric patches are then connected by coating a thin insulator layer with a conductive composite layer on the top. The whole composite coating can be easily installed on the surface like a paint. (If the substructure is non-conductive, a conductive sub-layer should be coated on the whole joint before attaching the piezoelectric patches.) When the structure is under dynamic deformation, electrical charge and voltage will be generated on surfaces of the piezoelectric patches due to the piezoelectric effect. The electric charge generated on the two piezoelectric patches should be different due to different responses and strain distributed at different positions of a structure. However, since the two piezoelectric patches are short connected, the electrical potential difference between them will be zero without crack or fracture. This leads to zero voltage reading in Figure 2-1. When damages occur at welding joint, the thin conductive coating will be broken synchronously. Therefore, the electrical field difference between the two patches can be noticed by the non-zero voltage reading. This indicates the happening of damage. The voltage difference between the two piezoelectric patches also presents the difference between the dynamic behaviors of two sides of the welding joint so as to possible indicate the local stiffness reduction, crack breathing induced bi-linearity or strain singularity at the crack tip. The damage severity increment and the potential of the crack propagation can be then estimated. Since the crack may occur on both welding edges, and we cannot predict which side of the weldment will the crack happens. A third piezoelectric patch (piezo-layer III shown in Figure 2-1) will be attached to the substructure on the further side of the weldment to localize the possible crack.

On the other hand, the FCF method is more sensitive to the vibration signal changes when breathing crack occurs, so two piezoelectric sensors can be applied on two sides of the welding joint. As a result, the third sensor can be eliminated, if only one crack occurs at the weldment. The Figure 2-1 (b) shows the sensor optimization for this method.

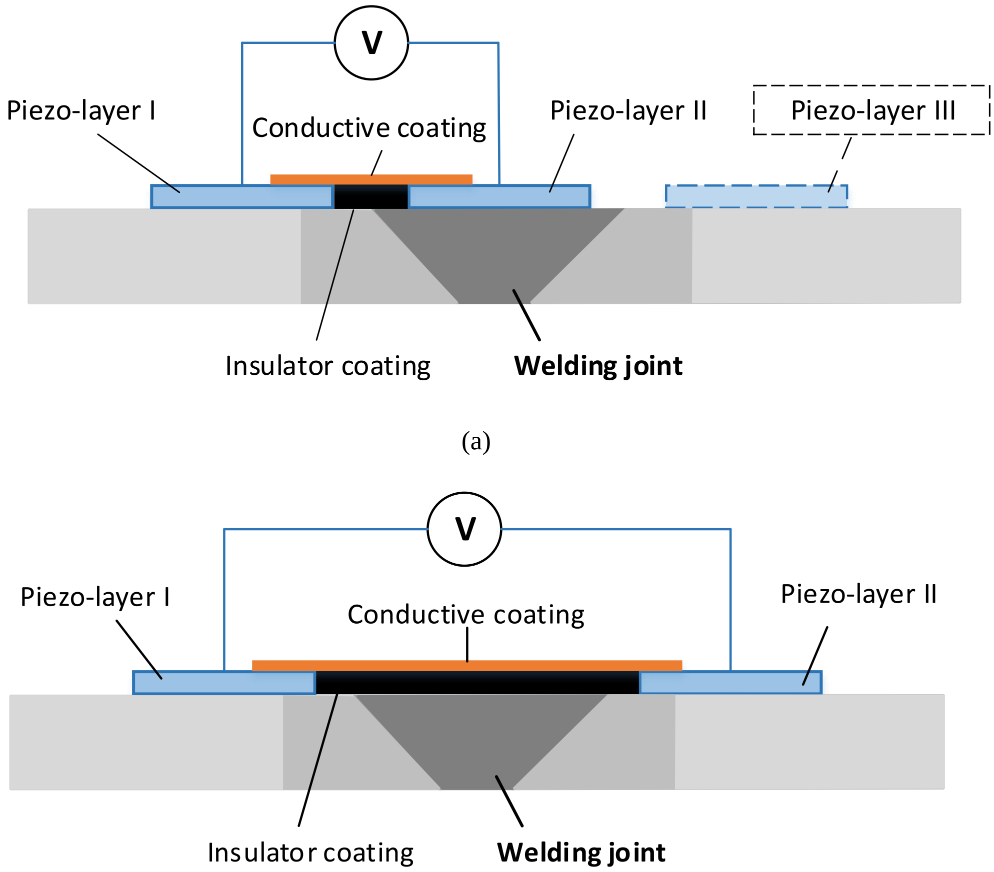

(a)

(b)

Figure 2-1. Composition of the piezoelectric coating sensor. (a) applied in the WT Sample Entropy Method; (b) applied in the FCF Method.

A wireless data transmission system can be introduced to upload signals from the smart coating with possible damage information to an internet database server in real-time [18]. Diagram of the whole onboard real-time damage detection system is provided in Figure 2-2. Detailed wireless module design and self-powering process are proposed and discussed in reference [18]. Analysis methodology of dynamic signals from the piezoelectric patches after crack happening by entropy is presented in the following section. Moreover, the piezoelectric patches and coating materials of the sensor were both tested in our lab and on a ground vehicle structure in an industry environment for 4 months. The sensor materials are proven to be sensitive to detect damages and durable.

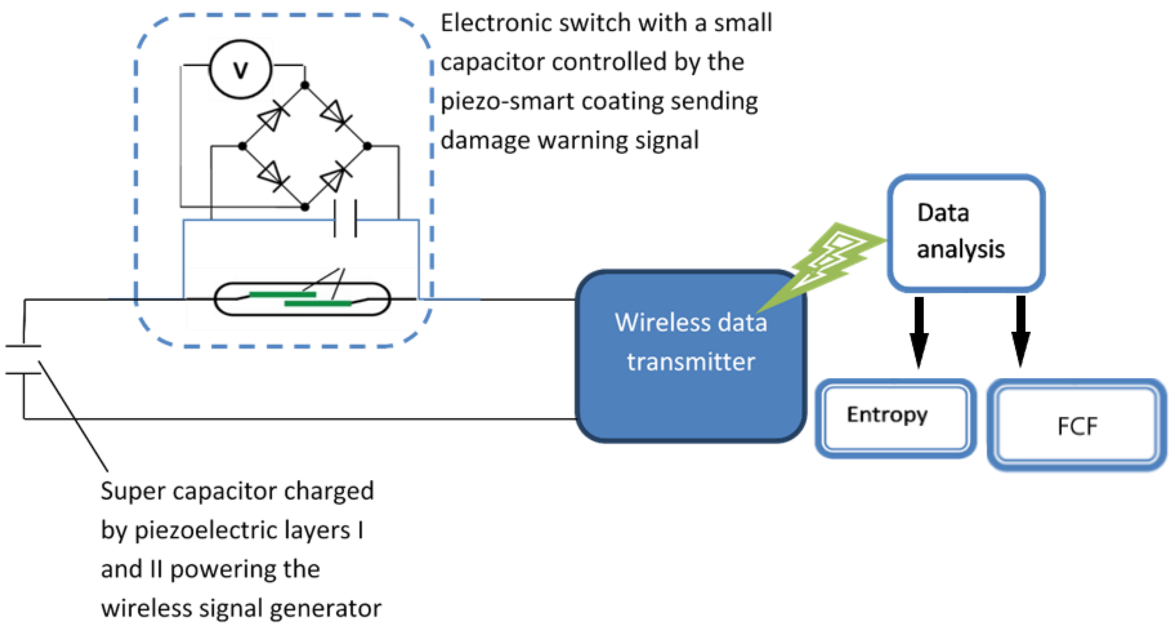

Figure 2-2. Block diagram of the whole on-board damage detection system referring [18]

2.2. WT Sample Entropy Measurement

In order to address the operating principle of crack identification with entropy, I need to discuss damage effects on dynamic response first. The breathing phenomenon of closed fatigue cracks produces the repetitive crack opening/closing and the variation of the structure stiffness during the vibration, which leads to weak bi-linearity in the dynamic response of the beam. Secondly, during the dynamic structural deformation, different levels of strain concentration always occur at the locations with geometry singularity, such as the crack tips for both close and open cracks. These lead to local material nonlinearity at the crack area and weak nonlinearity in the dynamic response. These nonlinearities can impose weak irregularities/perturbations in the vibration signals, which can be measured by the entropy value. Entropy is actually a measure of crack severity since these irregularities are directly related to the crack size and level of the strain concentration at the crack area.

Sample Entropy (SampEn) is not sensitive to the environmental noises. Hence, it was used to measure the irregularity of time domain signals so as to detect and evaluate the existing breathing crack for the first time [50]. In the thesis, I extend the crack identification to both open and closed cracks and introduce SampEn measurement to my work.

Let's take a time series X having N number of data points such as: $\{x(1), x(2), \ldots., x(N)\}$ then its irregularity can be calculated as follows.

First, template vectors of length m ('m' is called embedding dimension) are defined,

$$X(1) = \{x(1), x(2), \cdots, x(m)\}$$

$$X(2) = \{x(2), x(3), \cdots, x(m+1)\}$$

$$\cdots$$

$$X(N-m+1) = \{x(N-m+1), x(N-m+2), \ldots x(N)\}\,. \quad (2\text{-}1)$$

Then the Chebyshev distance between all template vectors are calculated, and let's denote it by $d[X_m(i), X_m(j)]$ and $i \neq j$. Then a parameter $B_i^m(r)$ is defined as follows,

$$B_i^m(r) = \frac{\#\ of\ j\ such\ that\ d[X_m(i), X_m(j)] \leq r}{N-m-1};\ (1 \leq j \leq N-m, j \neq i), \quad (2\text{-}2)$$

where r is a pre-determined tolerance value taken as:

$$r = k \times SD(X). \quad (2\text{-}3)$$

In Equation (2-3), k is a constant (k>0) and SD stands for the standard deviation. Then,

$$B^m(r) = (N-m)^{-1} \sum_{i=1}^{N-m} B_i^m(r). \quad (2\text{-}4)$$

Similarly, for template vectors of length m+1, we can have

$$A_i^{m+1}(r) = \frac{\#\ of\ j\ such\ that\ d[X_{m+1}(i), X_{m+1}(j)] \leq r}{N-m-1}; (1 \leq j \leq N-m, j \neq i). \qquad \text{(2-5)}$$

Similar to Equation (2-4), equation 2-5 can be re-written as,

$$A^{m+1}(r) = (N-m)^{-1} \sum_{i=1}^{N-m} A_i^{m+1}(r). \qquad \text{(2-6)}$$

SampEn is then defined as:

$$SampEn(m, r, N) = -\ln\left[\frac{A^{m+1}(r)}{B^m(r)}\right]. \qquad \text{(2-7)}$$

In this derivation, $B^m(r)$ is the probability that two vectors match with m points, on the other hand, $A^{m+1}(r)$ is the probability of the vector match with $m+1$ points. Therefore, the quantity $[A^{m+1}(r)/B^m(r)]$ is the conditional probability that two vectors with m points match with each other and remain within r tolerance at the next point [58]. Higher the irregularity of the time series, lower this conditional probability is. Hence, a higher SampEn value is obtained.

Besides, entropy itself is not sufficient enough to correlate the severity of the crack because of the weak signatures of the irregularities/perturbations generated by the breathing and material nonlinearity at small cracks. Wavelet transform (WT), which can magnify the perturbations or irregularities in signals [48], is hence introduced to further enhance the entropy measurement of the signal perturbations with higher sensitivity. Once these weak perturbations are magnified by using WT, the irregularities can be easily assessed using the entropy so as to evaluate crack breathing of closed cracks, strain concentration of closed and open cracks, and crack severity.

.

Wavelet transform is a smooth and quickly vanishing oscillating function. It maps a temporal signal, $f(t)$, into two-dimensional domain (the time-scale plane) and is denoted by $W_f(a,b)$ given by;

$$W_f(a,b) = \frac{1}{\sqrt{a}} \int_{-\infty}^{+\infty} f(t)\, h^*\left(\frac{t-b}{a}\right) dt = \int_{-\infty}^{+\infty} f(t)\, h_{ab}^*(t)\, dt, \tag{2-8}$$

where $h(t)$ is called the mother wavelet function and the subscript * denotes the complex conjugate of this function. The basis functions of the transform, called daughter wavelets, are given by;

$$h_{ab}(t) = \frac{1}{\sqrt{a}} h\left(\frac{t-b}{a}\right) dt, \tag{2-9}$$

$h_{ab}(t)$ is the wavelet obtained from the mother wavelet $h(t)$ by compression or dilation using scaling parameter a and temporal translation using shift parameter b [81].

2.3. Frequency Comparison Function (FCF) Method

It is known that the Frequency Response Function (FRF) is a mathematical representation of the relationship between the input and the output of a system [82]. FRF is a complex function which contains both amplitude (the ratio of the input force to the response) and phase (in degrees, which indicates whether the response moves in and out of phase with the input). Any function that contains amplitude and phase parts can be transformed into real and imaginary parts, and transformation equations are as below:

$$\text{amplitude} = \sqrt{real^2 + imag^2} \tag{2-10}$$

$$\text{phase} = tan^{-1}\left(\frac{imag}{real}\right), \tag{2-11}$$

where, the real part of the FRF equals zero at natural/resonant frequencies; and there will be 'peaks' in the imaginary part either above or below zero which indicate resonant frequencies.

In nomenclature, H represents the FRF in general. And the input is X, output is Y. Thus, the FRF is the cross-power (S_{xy}) of the input (x) and output (y) divided by the auto-power (S_{xx}) of input,

$$H = \frac{S_{xy}}{S_{xx}}. \tag{2-12}$$

For a dynamic response analysis, FRF is usually applied to present the nature of a vibration system, like natural frequencies, damping effects, and mode shapes, under different variable inputs and loading conditions. In my research, if I consider the dynamic signal of the left-side of the welding joint (piezo-layer I shown in figure 2-1) as an 'input' in FRF to its right-side structure, and the vibration signal close to the right side of the joint as a 'response'. The response function in equation 2-12 can present the dynamic natures of the local structure as well, including the possible crack induced nonlinearities. Herein, by mounting two piezoelectric layers at different locations of the tested vibrating structure, as shown in figure 2-1, two vibration responses can be recorded. In this study, FRF transforms into FCF. Subsequently, it presents a mathematical relationship between the two output signals recorded from the two piezo-patches (as shown in figure 2-1) of the vibrating beam on two sides of the welding joint. Meanwhile, it captures the dynamic nature of the local joint. When the structure is healthy, or a tiny crack happens to the welding joint, the beam is a linear vibration system. And the vibration signals on two sides of the joint will be very close to each other with the same frequency components but just tiny different amplitudes. In this case, we will hence have very low FCF standard deviation comparing the signals on two sides of the joint in the frequency domain. On the other hand, when a larger crack occurs at the welding joint, the vibration signals on both sides of the joint will have the nonlinear components. They can be different due to the nonlinear connection between the two patches, leading to higher standard deviation of the FCF in the frequency domain.

Based on the Equation (2-12), the basic formula for an FCF is,

$$H_C(f) = \frac{Y_2(f)}{Y_1(f)}, \tag{2-13}$$

where $H_C(f)$ is a FCF. $Y_1(f)$ is a output collected from the first point of the structure in the frequency domain, and $Y_2(f)$ is a frequency domain dynamic signal from the second location of the tested structure.

It is generally known that FRFs are most commonly used for response and excitation signals analysis with the calculation of the $H1(f)$ or $H2(f)$ FRF. These are extensively used for hammer impact analysis or resonance analysis. Similar to the FRFs, the FCF of $H1_c(f)$ is used in situations where $Y_2(f)$ in the system is expected to be relatively noisy comparing to $Y_1(f)$, and the FCF of $H2_c(f)$ is used in situations where $Y_1(f)$ in the system is expected to be relatively noisy comparing to $Y_2(f)$. And the equation of $H1_c(f)$ is as follow,

$$H1_c(f) = \frac{S_{y_1 y_2}(f)}{S_{y_1 y_1}(f)}, \tag{2-14}$$

where $H1_c(f)$ is a frequency comparison function, $S_{y_1 y_2}(f)$ is the Cross Spectral Density in the frequency domain of $Y_1(f)$ and $Y_2(f)$, where $S_{y_1 y_1}(f)$ is the Auto Spectral Density in the frequency domain of $Y_1(f)$. The FCF with basic terms can be described as

$$H1_c(f) = \frac{Cross\ Spectral\ of\ the\ output\ 1\ and\ Output\ 2}{Spectral\ Density\ of\ theoutput\ 1}. \tag{2-15}$$

The equation of $H2_c(f)$ therefore is as follows,

$$H2_c(f) = \frac{S_{y_2 y_2}(f)}{S_{y_2 y_1}(f)}, \tag{2-16}$$

where $H2_c(f)$ is a frequency response function, $S_{y_2 y_1}(f)$ is the Cross Spectral Density in the frequency domain of $Y_2(f)$ and $Y_1(f)$, and where $S_{y_2 y_2}(f)$ is the Auto Spectral Density in the frequency domain of $Y_2(f)$. the FCF with basic terms can be described as

$$H2_c(f) = \frac{Spectral\ Density\ of\ the\ output\ 2}{Cross\ Spectral\ of\ theoutput\ 1\ and\ Output\ 2}. \tag{2-17}$$

3. CRACK IDENTIFICATION WITH WT SAMPEN METHOD

3.1. Simulation Studies and Discussion

In this section, simulation process conducted in ANSYS software to obtain vibration signals of the cracked beam is explained in detail first, then crack severity increment is estimated in Matlab software using SampEn. Results are discussed in groups for open cracks and closed cracks, respectively.

3.1.1. FEM simulations

A vibrating welded beam with a crack (at the welding joint) is studied in FEM as a case study including the new smart coating. A schematic diagram with detailed dimensions and boundary conditions of the beam structure is shown in Figure 3-1. The beam is considered as a stainless steel 316 beam of a unit length (in meters) with a welding joint (butt weld) near the fixed end. Severe thermal changes occur to the base material (BM) during the welding process, and this thermal excursion experienced by the weldment varies from region to region. Three distinct zones with different material properties, which are base metal (BM), fusion zone (FZ) and heat-affected zone (HAZ), are generated in the weldment. The emphasis of the welding joint is also shown in Figure 3-1. In this study, the crack occurs on the top surface of the beam along the boundary between FZ and HAZ, and both piezoelectric patches are applied on the top surface of the structure. However, they can be used on both surfaces of the structure easily through a conductive metal bond.

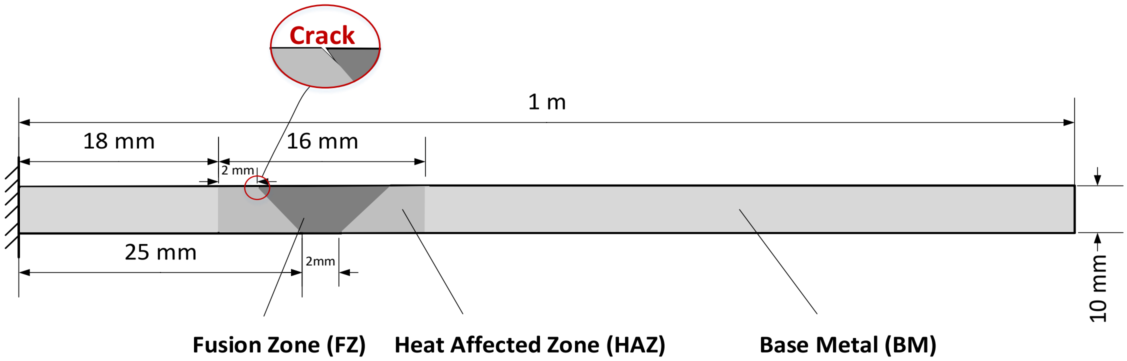

Figure 3-1. Welded cantilever beam with an open crack in the welding joint. (The dimensions are given for one case study.)

A finite element analysis (FEA) is established in Ansys 18.0 to simulate the beam vibration under base motion excitations and the generated signal from the piezo-composite coating. Figure 3-2 illustrates the FEM of the beam with the zoomed-in weldment area. The dimensions of the welded beam are shown in Figure 3-1 for a case study. For the piezoelectric patches, the length is 10 mm, and the thickness is 0.5 mm. Different material properties are preset to define different zones of the welded beam, and they are obtained from experimental testing [83] and given in Table 3-1. The material properties of the piezoelectric patches are shown in Table 3-2. The multi-linear material property of stainless steel 316 is considered and preset to define the material property at the crack tip. It simulates the nonlinear material property considering strain concentration/singularity. The parameters of the multi-linear property are determined by referring [84] and given in Table 3-3. Meanwhile, a contact pair is added to the crack walls to simulate the possible crack breathing during vibration. Plane elements 83 and 183 are used to mesh the crack tip area considering material nonlinearity and the host beam, respectively. Plane element 223 is used to mesh the piezoelectric patches considering the piezoelectricity. And the fine mesh is applied to the crack tip with the level of refinement set as 1 in ANSYS APDL.

After modeling, modal analysis is first conducted to obtain the natural frequencies of the structure. In this case study, the first three natural frequencies are around 52.59 rad/s, 329.26 rad/s, 920.93 rad/s, respectively. Then, the base motion excitation frequency during the transient analysis is decided to be away from the first natural frequency as 49 rad/s so as to avoid the resonance with reasonable deflection. During the transient analysis process, the end close to the welding joint is fixed along the beam direction (X direction). Meanwhile, harmonic base motion along the direction perpendicular to the beam (Y direction) with variable amplitudes is applied for this case study with the fixed frequency of 49 rad/s. Considering the vibration close to the first mode, damping effect is considered in the simulations with an equivalent damping ratio of 1%. Convergence study of the simulation step length and data numbers in 5 s simulation period is shown in Figure 3-3. The step length for transient analysis changes from 5 ms to 0.5 ms with data number varying from 1000 to 10000. It is noted that the entropy value changes from 0.29 to 0.072 when the step length reduced from 5 ms to 0.5 ms. And the entropy value convergences at 1 ms step length with around only 5% difference with the one at 0.5 ms. Therefore, to balance the simulation cost and crack identification accuracy, the vibration signal is obtained with a time interval of 0.001s by 5 s simulation period in my FEA.

Table 3-1. The material properties of the welded beam [83]

Type	Young’s Modulus (GPa)	Poisson’s ratio
Heat Affected Zone	278	0.35
Base Metal	211	0.31
Fusion Zone	200	0.3

Table 3-2. The material properties of the piezoelectric patches

Parameters	Piezoelectric patches
Young’s modulus (GPa)	78

Mass density (kg/m^3)	7.6×10^3
e_{31} (C/m^2)	-5.4
d_{31} (C/N)	-1.71×10^{10}
C_v (nF)	2.3541 for a piezoelectric patch with a dimension of 0.01 m × 0.07 m × 0.0005 m.

Table 3-3. Multilinear material property of stainless steel 316 [84]

Linear Elasticity	**Young's Modulus (GPa)**	**Poisson's ratio**
	211	0.31
Multilinear elasticity	**Strain (0.001)**	**Stress (Mpa)**
	1.04	175
	1.56	200
	2.08	205
	2.70	211
	3.02	213

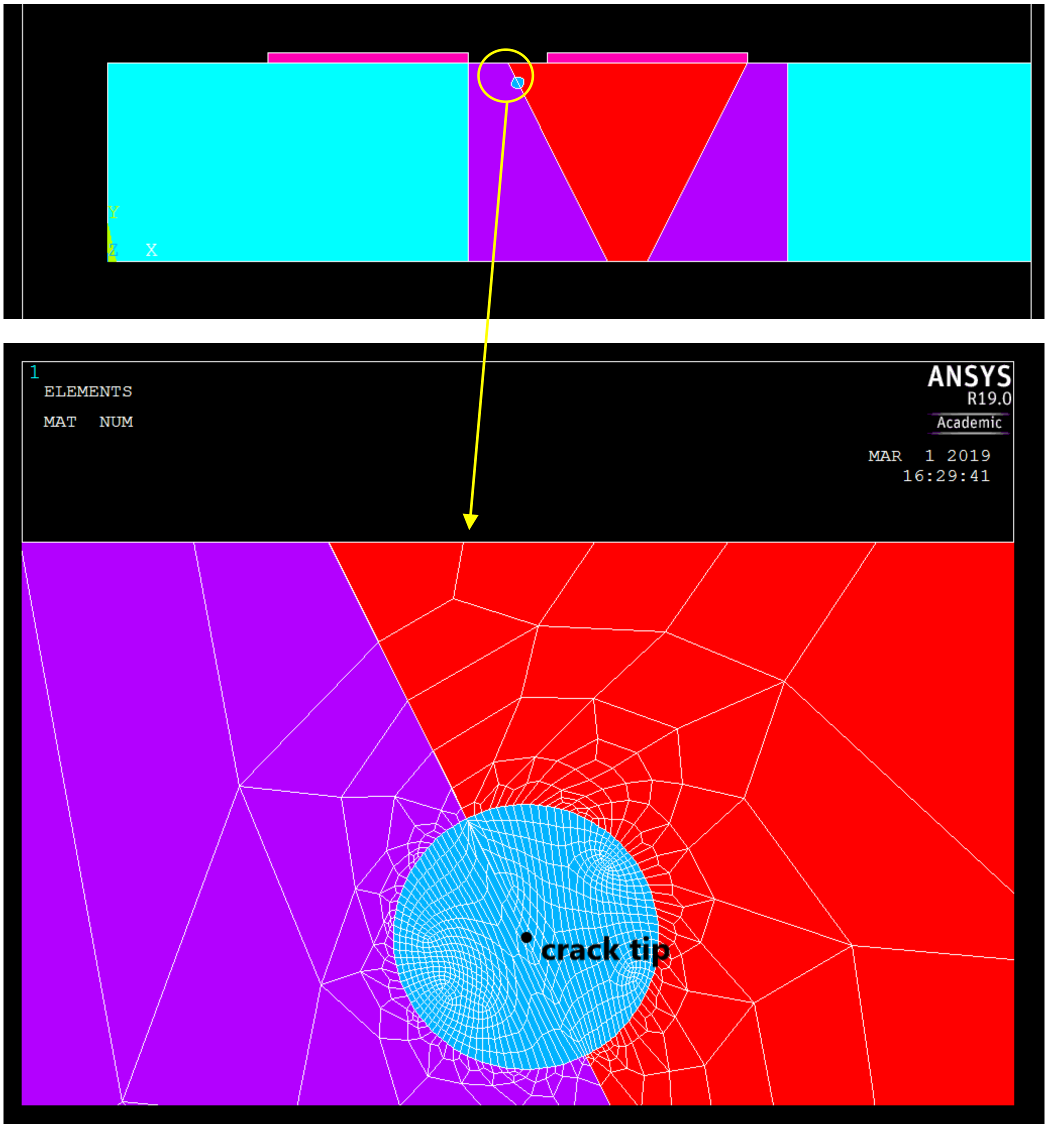

Figure 3-2. The zoom-in finite element model of the crack identification module located at a welding joint of the beam (the crack is 10% depth of the beam thickness, and a closed crack is shown in this figure considering contact pair between crack walls).

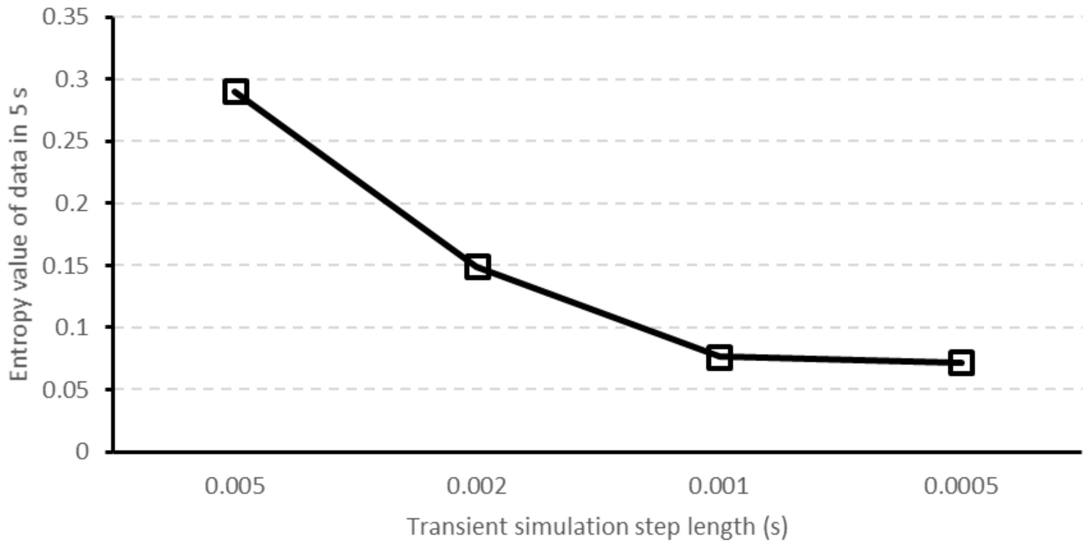

Figure 3-3. Convergence study of step length and data number in FEM transient analysis

In the study, two significant factors for crack identification are crack breathing and material nonlinearity at the crack tip. Models with open crack are also established by increasing the distance between two crack walls to simulate the cracks only considering material nonlinearity.

3.1.2. Numerical results and discussion

In this case study, two variables during FEM simulations are the base motion amplitude and the crack depth. Hence, the results generated by the simulation process are separated into two main groups: group 1 with the same crack depth (10% of the beam thickness) but different strain concentration levels at the crack tip with different base motion excitation amplitudes (increases from 0.0015 m to 0.0055 m); group 2 with the same excitation (amplitude of 0.005 m and frequency of 49 rad/s) but different crack depths (increases from 5% to 15% of the beam thickness). Considering consistency in the modeling process, for group 1, I use the same beam model but apply different base motion amplitudes along the fixed end of the cantilever beam. For group 2, the beam models change slightly with increasing crack depth. But the meshing configurations at the crack tips are the same in those different models, and for the rest part of the cantilever beam, meshing is quite similar. Since a regular meshing is good enough to provide accurate strain distribution if there is no crack and geometry singularity at the weldment, the meshing configuration at the welding joint for a healthy beam is different from a damaged one. But the meshing of the rest part of the beam is the same with other damaged beam models.

Time-domain signals are generated from the FEM transient analysis. Figure 3-4 shows the vibration responses of both the healthy beam and the damaged beam at the piezo-layer I and the piezo-layer II, and their comparison as well. The excitations applied to both beams are the same with a harmonic base motion with a 0.005 m amplitude. and the crack of the damaged beam is a 10% depth closed crack in Figure 3-4 as an example to present how these simulated signals differ from each other. Then, time-domain signals are analyzed with Wavelet SampEn algorithm coded in Matlab®. As illustrated in the 2.2, SampEn is defined as: $SampEn(m, r, N) = -\ln\left[\frac{A^{m+1}(r)}{B^{m}(r)}\right]$. It employs two parametric values during the analysis process: embedding dimension (m) and k value, which varies the tolerance value (r) (Equation 2-3). In this study, the parameters for SampEn are hence set to be m = 2 and k = 0.2 following the values used in [50]. As long as the same parameters in Entropy calculation are used, the relative Entropy value compared with the healthy case will correctly show the damage severity. Before SampEn calculation, I apply wavelet transform and use the translation factor as a varying 'location' in the time domain to scan the whole sampled signal. In the algorithm, 'symlet2' is used as the mother wavelet function and WT is realized by a Matlab code, which 'Scale' is an input argument to determine the degree to which the wavelet is compressed or stretched. I also introduce another argument 'Repeat' to determine the repetition times of the wavelet transform to gain the best perturbation magnification effect. So, 'Scale' and 'Repeat' are two parameters in the algorithm for WT process. It is found that these parameters have a more significant influence on the final entropy values and crack identification sensitivity during the analysis. The entropy values with respect to different 'Scale' and 'Repeat' are observed using a three-dimensional plot (3D plot). Figure 3-5 (a) is graphed for the entropy values based on the vibration signals generated by the piezo-coating of the welded beam with a closed crack of 10% depth of the beam thickness and base motion amplitude of 0.005 m and frequency of 49 rad/s. For Figure 3-5 (b), the crack in the welded beam model is set as an open crack with the same size by considering the nonlinear material property at the crack tip with the same size of the crack and excitation used in Figure 3-5 (a). After optimization, the 'Scale' is set as 10, and 'Repeat' is set as 9 when considering only crack breathing, meanwhile, 'Scale' as 5 and 'Repeat' as 6 when considering only material nonlinearity at the crack tip.

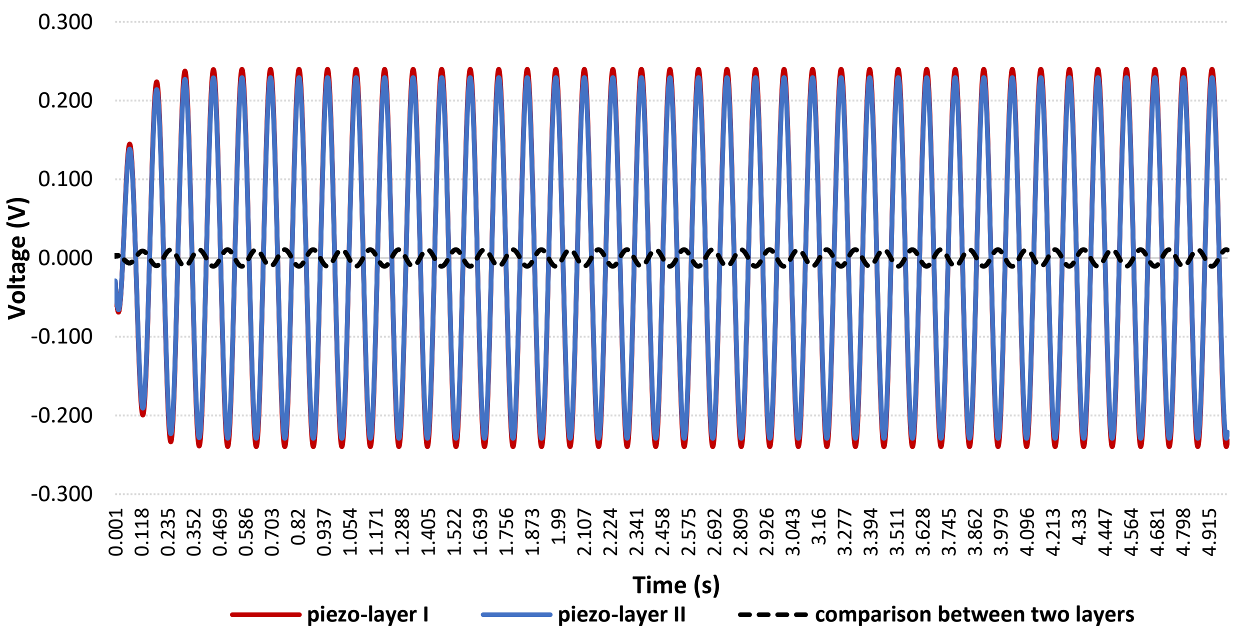

(a)

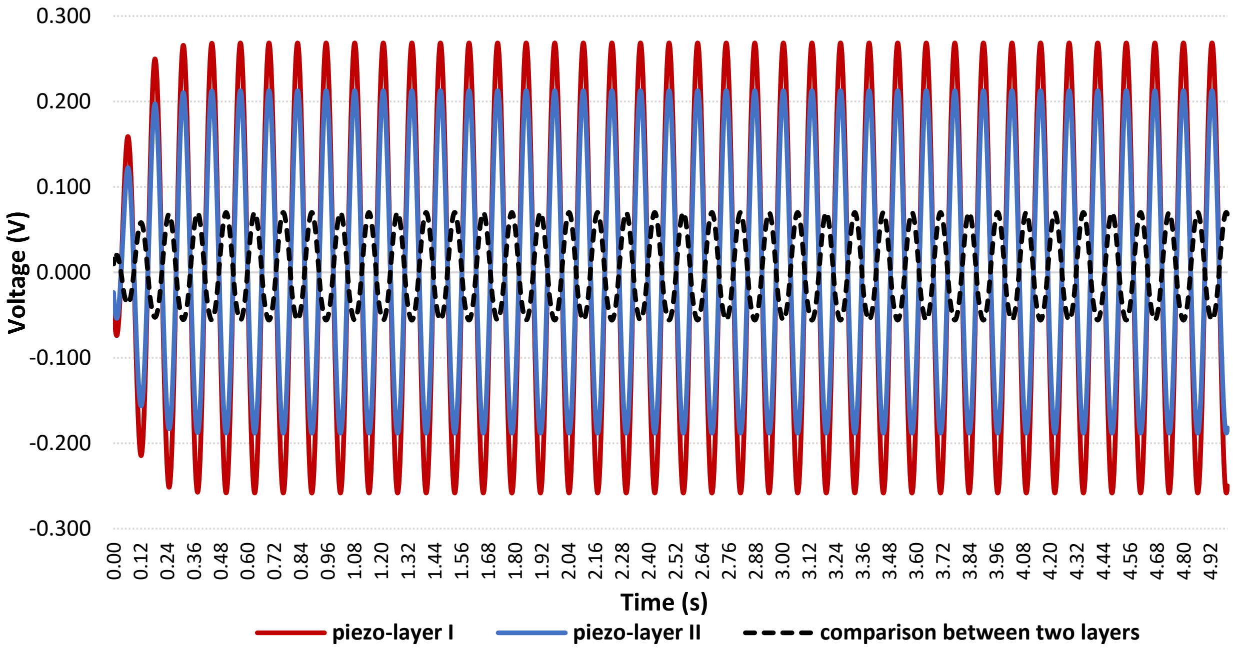

(b)

Figure 3-4. (a) Voltage signals generated from the simulation of a healthy beam (with broken coating); (b) Voltage signals generated from the simulation of the damaged beam with a crack of 10% of the beam thickness. Both beams are under excitation of harmonic base motion with 0.005 m amplitude and 49 Rad/s frequency.

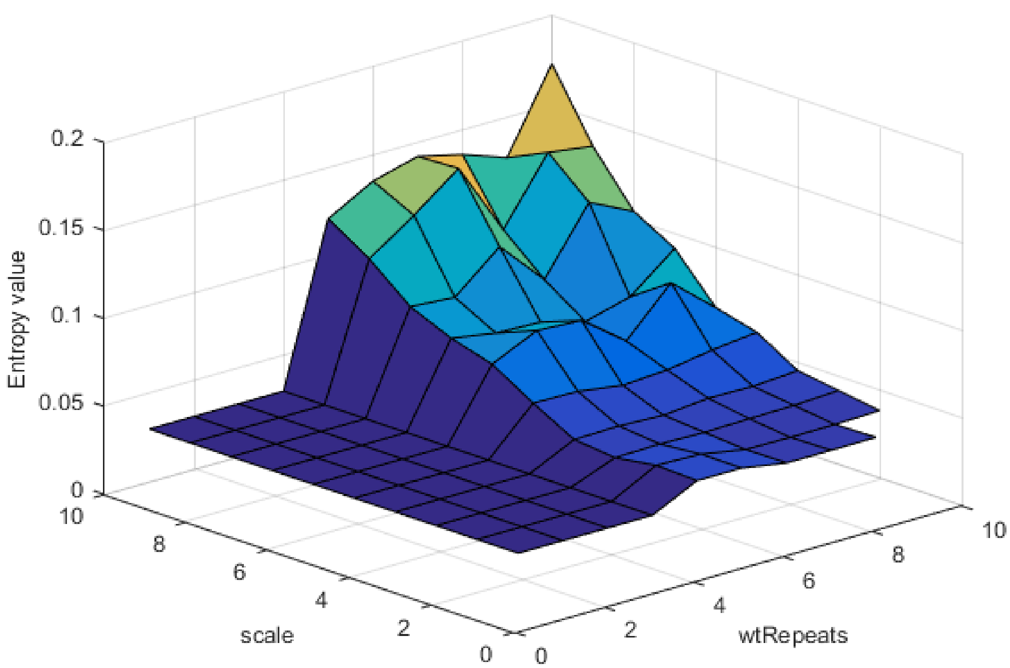

(a)

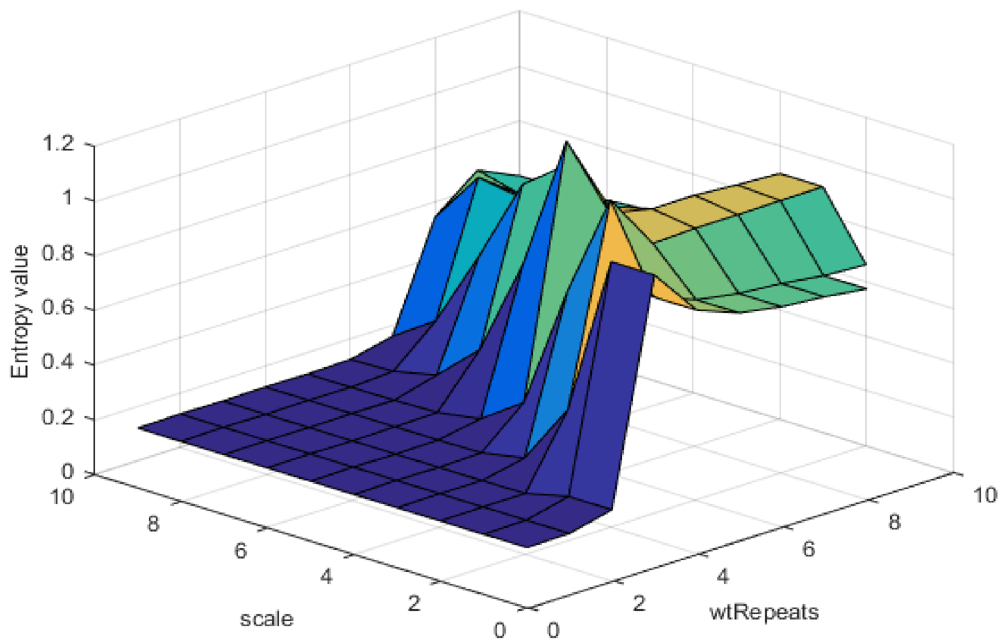

(b)

Figure 3-5. (a) WT optimization considering only crack breathing; (b) WT optimization considering only strain concentration and material nonlinearity at the crack tip. Crack is 10% depth of the beam thickness with excitation amplitude of 0.005 m and frequency of 49 rad/s.

According to the two charts in Figure 3-5, for the damaged beam with a crack of relatively low crack depth as 10% of the beam thickness, entropy value is relatively small as no more than 0.2 when only considering crack breathing. But entropy value becomes higher (around 1.2) when considering only strain concentration and material nonlinearity at the crack tip. The main reason is that when the damage is an open crack, white noise from FEM simulations magnified by WT is found to be more significant. In this case, I set a perfect harmonic sinusoid wave as the input signal to a beam with no crack and use the entropy value generated from its dynamics signal as the healthy state entropy.

As mentioned before, the results of this research are separated into two groups. For group 1: the crack depth is fixed at 10% of the beam thickness, but the base motion amplitude is varied from 0.0015 m to 0.0055 m. In this case, the von Mises strain at the crack tip increases with increasing of the base motion amplitude. I set the von Mises strain level at the crack tip as the independent variable.

Figure 3-6 (a) and Figure 3-6 (b) show entropy variation ratio compared with the healthy structure under different crack tip strain levels considering only crack breathing and only strain concentration (material nonlinearity) at the crack tip, respectively. In Figure 3-6 (a), the crack is a closed crack considering breathing effect, and two parameters of WT are set as Scale of 10 and Repeat of 9. In this case, entropy value is as small as 0.0004 for the healthy beam using optimized SampEn algorithm (Scale = 10, Repeat = 9). Hence, the entropy variation ratio versus healthy structure becomes so high as almost 40000% when the von Mises strain level reaches 0.002869 from the piezo-layer II. It is noted the strain concentration level at crack tips obtained from my simulation also indicates the area of the materials with nonlinearity, which affects the perturbation in the vibration signal as well. This area is covered by the one modelling material nonlinearity in FEM. For the piezo-layer II, the entropy variation ratio increases from 18900% to 31100% as the strain level increases from 0.00078 to 0.001304. Then it shows a relatively constant trend as the strain level changes from 0.001304 to 0.00182. And the entropy ratio increases again from 30475% to 38675% as the strain level reaches 0.002869 at last. Meanwhile, the increasing trend becomes plat when the strain level reaches 0.002347. However, for the piezo-layer I, the entropy ratio increases from 550% to 17650% at first (the strain varies from 0.00078 to 0.00134) and keeps stable after the strain level at the crack tip reaches 0.001304. Compared between both piezo-layers, the entropy variation ratio based on the voltage between two piezo-layers shows a relatively steady growth trend which increases from 12550% to 39575% when the strain level increases from 0.00078 to 0.002869. However, the entropy variation is relatively smooth (varies from 37750% to 39575%) after the strain level at the crack tip reaches 0.001825.

In Figure 3-6 (b), the crack is an open crack considering material nonlinearity effect, and the parameters of WT are set as Scale of 5 and Repeat of 6 following the results in Figure 3-5. Compared with the high sensitivity shown in Figure 3-6 (a), the highest entropy variation ratio is nearly 800% as strain level of 0.001547 for the piezo-layer II. Meanwhile, with the increment of the strain level at the crack tip, both piezo-layers show a decreasing trend after the entropy variation reaches a maximum value. But the turning points are different for both piezo-layers. For the piezo-layer II, the entropy variation ratio increases from 348% to 779% when the strain at the crack tip increases from 0.000773 to 0.001547 and then decreases to 685% as the strain level changes to 0.00232. For the piezo-layer I, the turning point occurs when the strain level reaches 0.001289. At this point, the entropy ratio increases to 582% and then goes down to 355% when the strain increases to 0.00232. However, the entropy variation based on the voltage between the two piezo-layers shows a smooth increasing trend. The entropy variation ratio increases from 238% to 591% smoothly when the strain level at the crack tip changes from 0.000773 to 0.00232. To sum up, the signal of comparison between two layers indicates a relatively stable and reasonable increasing trend on both occasions in Fig. 8 so as to be more reliable for crack identification aim. For the open crack identification with entropy, good results can be obtained only if the voltage between two piezo-layers are used for the entropy calculation.

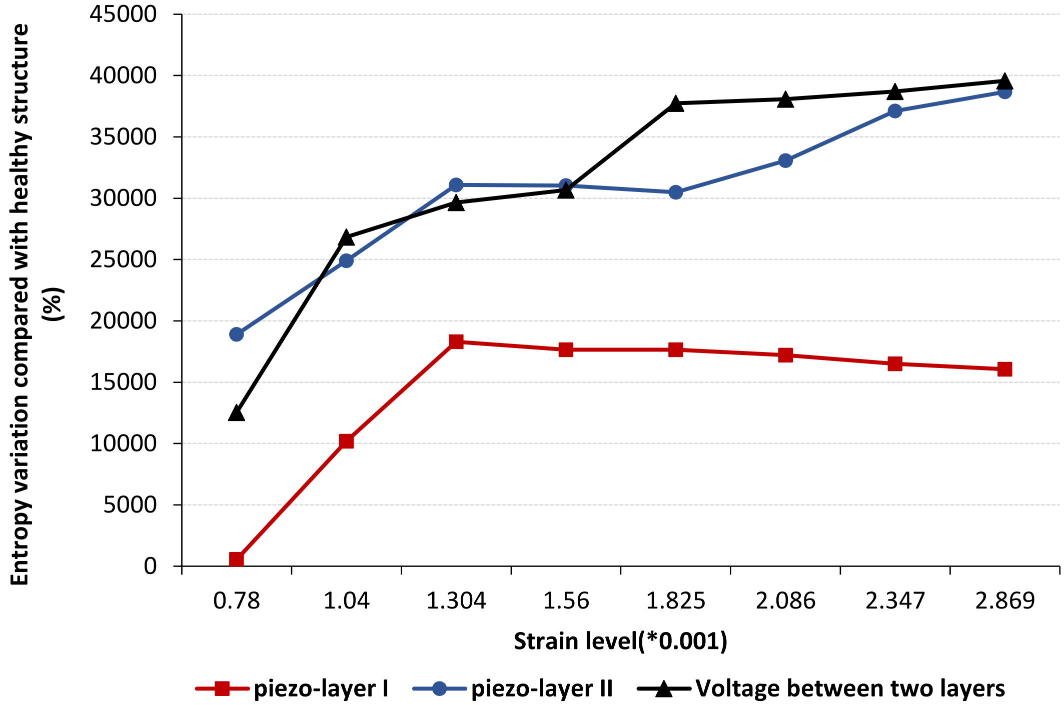
45000
40000
35000
30000
25000
20000
15000
10000
5000
0
Entropy variation compared with healthy structure (%)
0.78
1.04
1.304
1.56
1.825
2.086
2.347
2.869
Strain level(*0.001)
piezo-layer I
piezo-layer II
Voltage between two layers

(a)

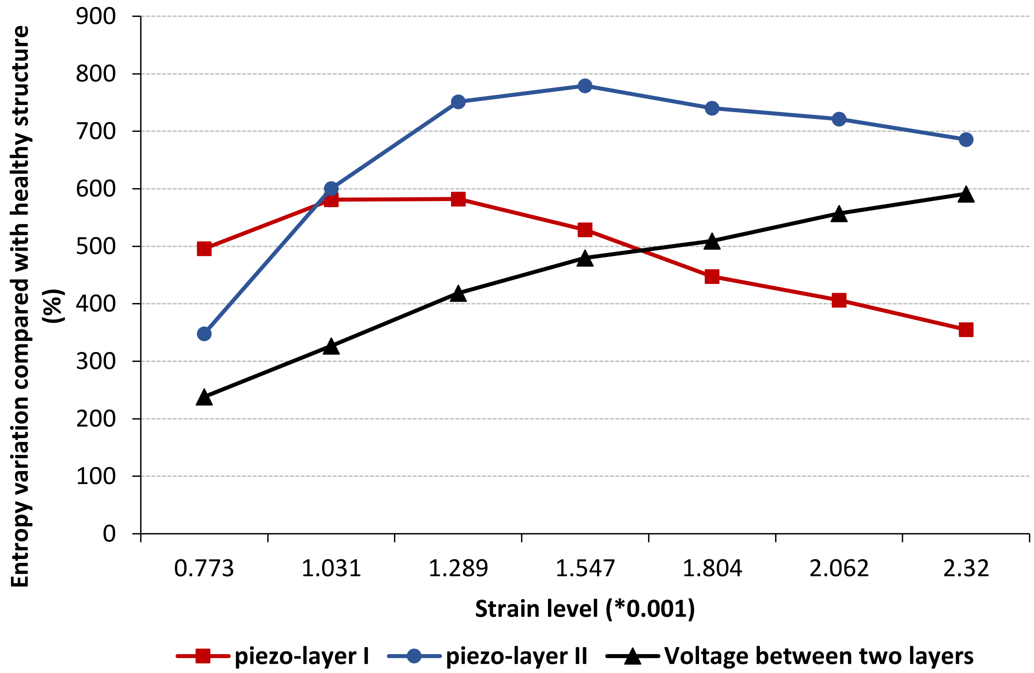
900
800
700
600
500
400
300
200
100
0
Entropy variation compared with healthy structure (%)
0.773
1.031
1.289
1.547
1.804
2.062
2.32
Strain level (*0.001)
piezo-layer I
piezo-layer II
Voltage between two layers

(b)

Figure 3-6. (a) Entropy variation versus different tip strain levels considering only crack breathing of a closed crack (Scale = 10, Repeat = 9); (b) Entropy variation versus different tip strain levels considering only strain concentration and material nonlinearity at crack tip (open crack, Scale = 5, Repeat = 6). Crack is 10% depth of the beam thickness with the frequency of 49 rad/s and increasing excitation amplitude.

Based on the findings from Figure 3-6, the entropy variation versus different tip strain levels considering both crack breathing and material nonlinearity is studied using two optimized WT algorisms, as shown in Figure 3-7. The beam model is the same as Figure 3-6 (a). First, I calculate the entropy value under two optimized WT separately and then sum up both entropy values to get the combined results. The calculation process is shown as follows,

$$\mathrm{SampEn(cracked\ beam)} = \{SampEn\ (WT\ coeff(5,6)) + SampEn(WT\ coeff(10,9))\}\ for\ cracked\ beam \quad (3\text{-}1a)$$

$$\mathrm{SampEn(healthy\ beam)} = \{SampEn\ (WT\ coeff(5,6)) + SampEn(WT\ coeff(10,9))\}\ for\ healthy\ beam \quad (3\text{-}1b)$$

$$\mathrm{SampEn\ variation\ percentage} = \frac{SampEn(cracked\ beam) - SampEn(healthy\ beam)}{SampEn(healthy\ beam)} * 100\%. \quad (3\text{-}2)$$

According to the graph in Figure 3-6, the entropy variation ratio shows a relatively bouncing trend along with the strain level change for the piezo-layer I. In the beginning, it increases from 11% to 753% when the strain at the crack tip changes from 0.00078 to 0.001304. And then the entropy variation ratio reaches the peak of 753% again when the strain level at the crack tip reaches to 0.001825. In the ranges before and after this point, the entropy ratio decreases at first and then increases slightly. For the piezo-layer II, the entropy ratio increases from 386% to 986% when the strain changes from 0.00078 to 0.00156, and then, it decreases to 894% when the strain increases to 0.001825. After that, it shows a relatively steady and flat increasing trend. More specifically, when the strain level reaches 0.002869, the entropy variation ratio versus healthy structure is

1061%. Similar to the piezo-layer II, the entropy variation based on the voltage between both piezo-layers increases from 258% to 1093% as the strain at the crack tip increases from 0.00078 to 0.002086. And then it reaches a relatively constant value (varies from 1093% to 1041%) with the increment of strain level higher than 0.002086. The comparison between two piezo-layers shows the smoothest variation trend in this case.

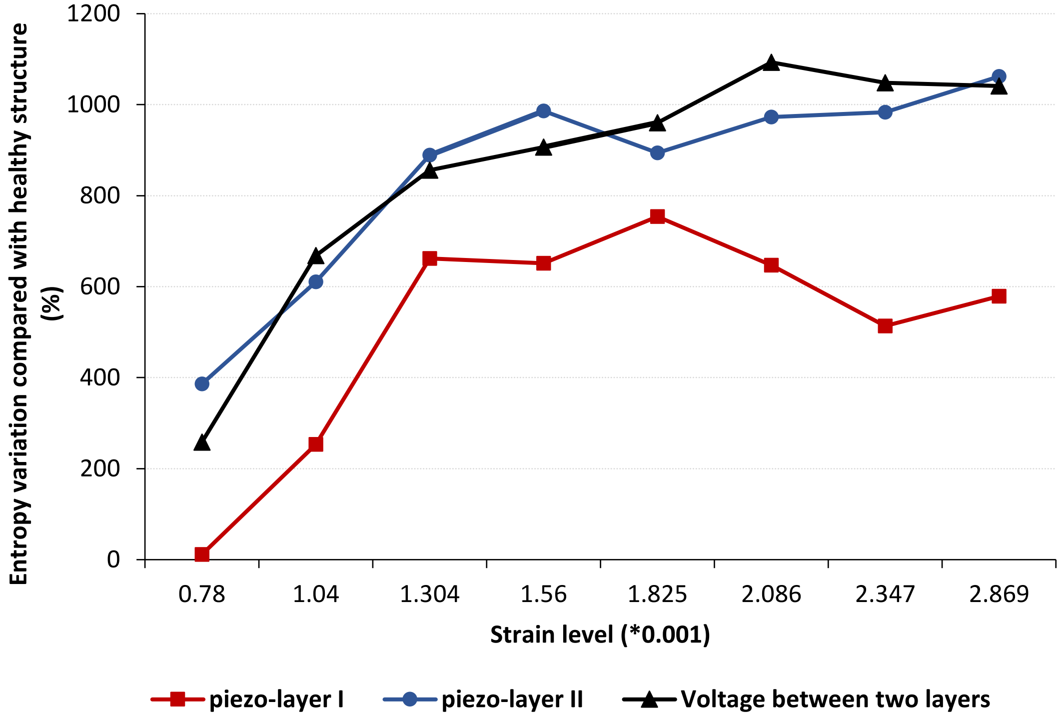

Figure 3-7. Entropy variation versus different tip strain levels considering both crack breathing and material nonlinearity (breathing crack) using two optimized algorisms (Combination of Entropy values with Scale = 10, Repeat = 9 and Scale = 5, Repeat = 6). Crack is 10% depth of the beam thickness with the frequency of 49 rad/s and increasing excitation amplitude.

Figure 3-8 shows the sensitivity of wavelet SampEn application on crack depth estimation. In this study, models with different crack depths are established to simulate the vibrating signals. The base motion conditions set for each simulation are the same harmonic sinusoidal motion (frequency = 49 rad/s, amplitude = 0.005 m). As shown in Figure 3-8, the piezo-layer I signal shows an inconsistent trend along with the increase of the crack depth. The entropy variation ratio increases from 370% to 613% in the beginning as the crack depth changes from 5% to 8%. It keeps a constant sensitivity in the crack depth range between 8% and 12% and then shows an abnormal upward trend from 610% to 900% when the crack depth increases from 12% to 15%. The entropy variation based on the voltage from the piezo-layer II and the voltage between both piezo-layers presents a similar reasonable trend. The entropy variation ratio of both voltages shows a sharply increasing trend when the crack depth is smaller than 10%, and the comparison shows a higher sensitivity in this crack depth range. The entropy variation ratio based on the voltage between both piezo-layers changes from 180% to 1071% when the crack depth increases from 5% to 10%, and the ratio changes from 316% to 1020% for the piezo-layer II in comparison.

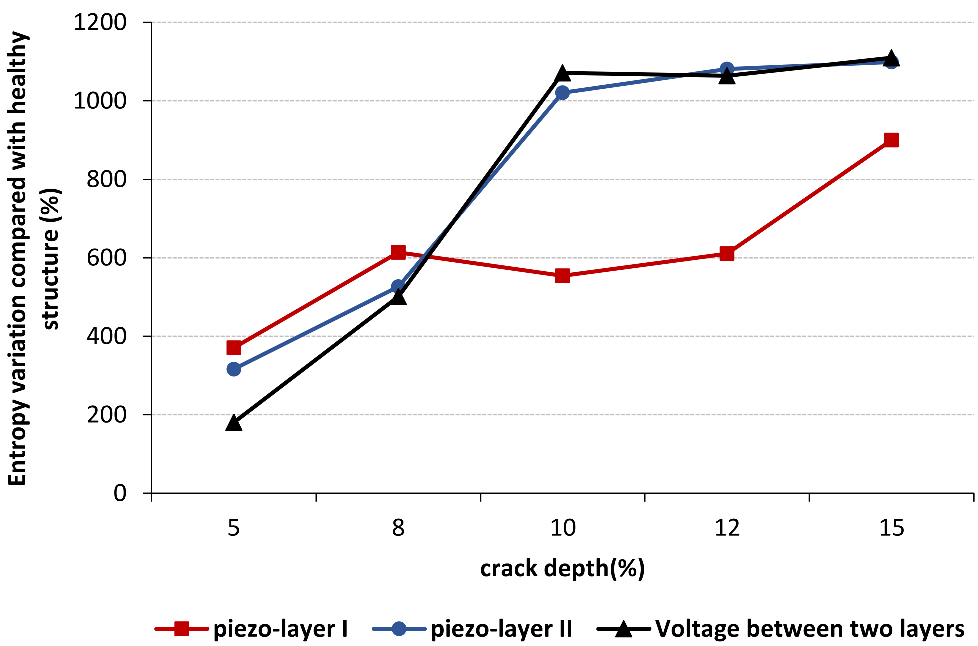

Figure 3-8. Entropy variation versus different crack depth with same excitation condition considering both crack breathing and nonlinearity (Entropy combination with Scale = 10, Repeat = 9 and Scale = 5, Repeat = 6). Base motion amplitude and frequency are 0.005 m and 49 rad/s, respectively.

In summary, with the new design of the piezoelectric coating sensor and the wavelet sample entropy measurement based on comparing voltage between two piezo-layers, I can obtain more consistent results with smoother entropy variation ratio trend both along with crack tip strain and crack depth increment.

3.1.3. A different case study

To validate the feasibility of the sensor design and the WT SampEn measurement application to other beam structures and to study the possibility of entropy calculation extending to beams with different sizes. I also do a group of simulations with a different welded beam model. For the new model, I increase the beam length from 1 m to 1.2 m. Meanwhile, I moved the welding joint away from the fixed end by 0.1 m along the beam length direction, and the size of the welding joint keeps the same.

The simulation process in ANSYS APDL is the same with the studies before, and I did the studies with the healthy beam model and the damaged beam with a 10% (of the beam thickness) open crack. I set a different excitation frequency as 28 rad/s. To be consistent with the strain level obtained in the case study above, I modified the base motion amplitude from 0.0055 m to 0.016. And the strain level at the crack tip increases from 0.00074 to 0.00215 accordingly to cover the linear and nonlinear material property ranges.

The entropy variation for the welded beam with an open crack compared with the healthy beam is shown in Figure 3-9. It is noted that before the WT SampEn calculation process, the WT optimization should be done first, and the optimized parameters for WT are 2 for scale and 3 for repeat in this case study. The WT optimization algorithm was embedded in the wavelet SampEn algorithm referring [50]. In Figure 3-9, the entropy variation ratios for both piezo-layers show a similar increasing trend from 1140% to 1160% when the strain level at the crack tip increases from 0.00074 to 0.00134. Then both ratios go down to 403% and 422% respectively when the strain level increases to 0.00215. On the other hand, the entropy variation ratio for the comparison voltage between two piezo-layers keeps a smooth increase trend from 979% to 1218% when the strain level goes up from 0.00074 to 0.00215. It furtherly confirms that only the comparison voltage between two piezo-layers can estimate the strain concentration increment and the potential crack propagation with an open crack. And the method is sensitive for the crack identification despite the size of the beam.

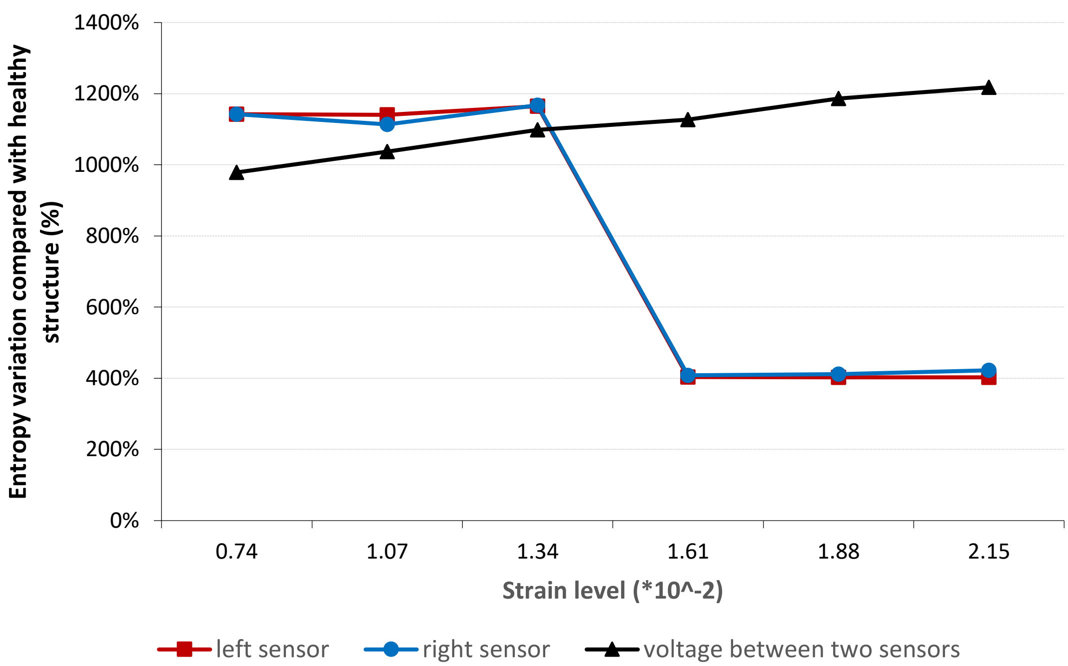

Figure 3-9. Simulation of the case study with a welded beam model with different size (beam length: 1.2 m): Entropy versus different tip strain levels considering only strain concentration and material nonlinearity at crack tip (open crack, Scale = 2, Repeat = 3). Crack is 10% depth of the beam thickness with the frequency of 28 rad/s and increasing excitation amplitude from 0.0055 m to 0.016 m.

Cracks with specific size and tip strain concentration at the welding joint on different structures, like plates and shells, may lead to different entropy variation. It is hard to quantify the exact crack size by a general/universe algorithm on different engineering structures at the current stage, and the crack identification for plates and shells considering three-dimensional strain distribution is one of my important future work.

3.2. Experimental Validation and Discussion

Experimental identification of breathing closed cracks (without considering strain singularity at the crack tip) with different crack depth on a beam has been realized by Entropy measurement [51]. In this section, experimental studies on identification of an open crack considering the different level of strain singularity at its tip are carried out to validate the results and conclusions from simulations. In experimental realization, there are some factors different from the simulation due to the experimental environment limitation. Firstly, the beam used in the experiment is made of aluminum since it is much easier for us to cut a crack with controllable size. The whole length for the beam is 2 m, and I set the middle point as the base motion point so that the length for the effective vibrating part is 1 m. Secondly, in the experiment, it is not a welded beam. However, the crack mechanism and its effect on the dynamic response are similar for beam models used in simulations and experiments. In the experimental study, I confirm the feasibility of the new sensor design and the methodology according to the variation trend concluded from the simulation results.

Figure 3-10 gives the experimental setup of the beam mounted with the smart coating according to the sensor design description in section 2.1. The lengths of the cracked beam and the piezoelectric patches are the same with simulations considering the factors explained in the previous paragraph. While the widths and thicknesses are 19 mm, 3 mm and 7 mm, 0.5 mm for the beam and the piezoelectric patches, respectively, based on the available parts in the lab. Again, although the thickness of the beam in the experiment is different from the one used in the simulation, the crack mechanics and effect on detection results will be the same. The aluminum beam mounted with the crack identification coating is attached to a shake provided by the Modal Shop Inc. (Model 2100E11 100lbf Modal Shaker) at the center of the beam, as shown in Figure 3-

10 (a). In order to be consistent with the simulations, meanwhile, to avoid the large deflection, which can break the thin piezoelectric patches, steady sinusoidal base motions with frequency of 5 Hz (close to the first natural frequency of the beam) and amplitudes of around 0.0005 m and 0.001 m along vertical direction are provided by the shaker. The data acquisition is done using the LMS SCADAS Mobile (type SCM05) data acquisition hardware which is integrated with the LMS Test.Lab software platform. Each piezoelectric patch is connected to the LMS. When the beam is vibrating, the voltage signal from the surface of the piezoelectric patch with a period of 4 s is captured by the LMS data acquisition system. Figure 3-11 shows the detailed installation of the smart coating. Figure 3-11 (a) indicates the healthy state of the beam, the voltage between two piezoelectric patches detected by the data acquisition software keeps 0 as shown in Figure 3-12 (a) since two patches are short connected. As shown in Figure 3-11 (b), the conductive layer is broken, which indicates the initial state of the crack generation. The voltage variation between the two piezoelectric patches can be noticed and shown in Figure 3-12 (b) with 0.0005 m base motion amplitude. For an open crack cut to nearly 10% depth of the beam thickness as shown in Figure 3-11 (c) and Figure 3-11 (d), the voltage signals of the two piezoelectric patches and the voltage comparison between two patches recorded by LMS with base motion amplitude of 0.0005m are presented in Figure 3-12 (c).

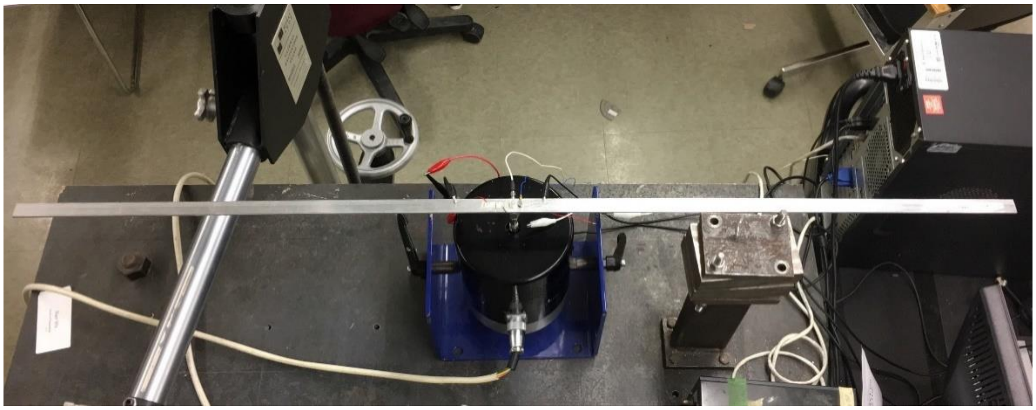

(a)

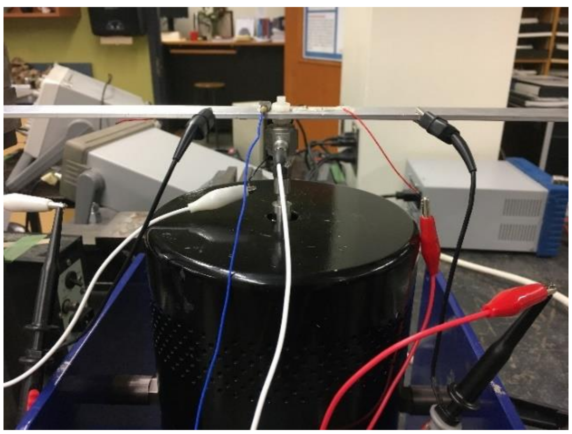 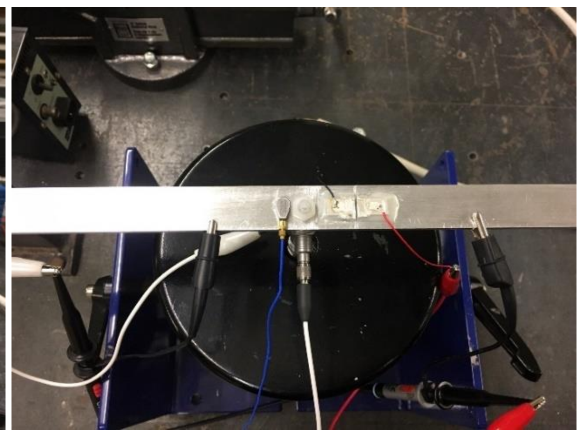

(b) (c)

Figure 3-10. (a) Overview of the whole experiment set up. (b) Front view of the beam set up which focus on the base motion point. (c) Top view of the beam set up which focus on the smart coating.

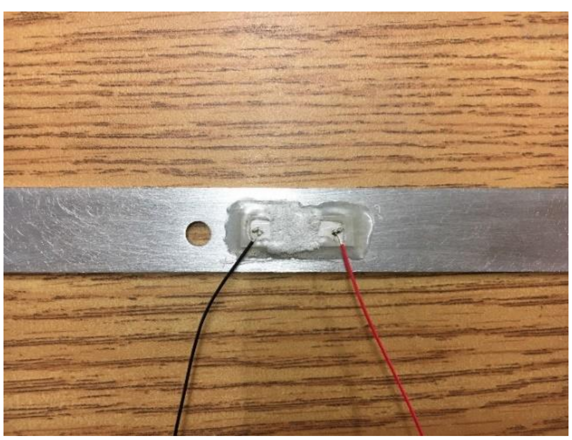 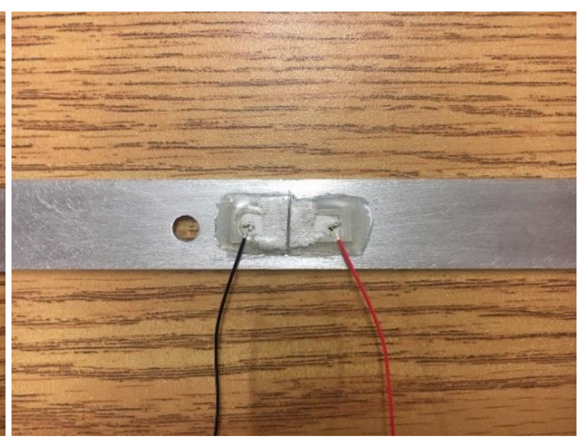

(a) (b)

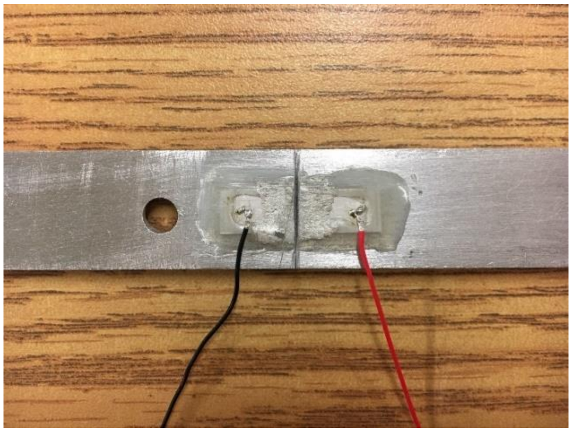

(c)

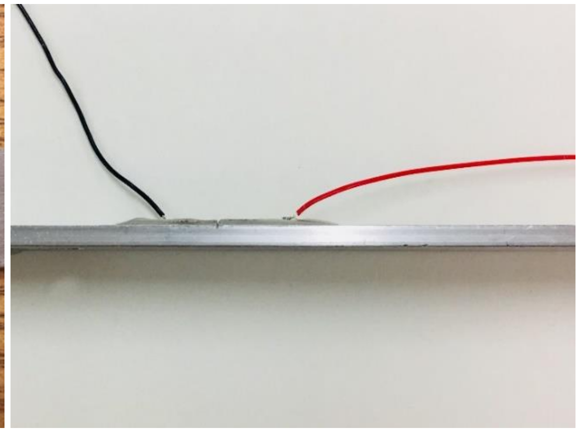

(d)

Figure 3-11. (a) Installation of the smart coating (beam with the intact coating). (b) Beam with the broken coating which indicates the beginning of the crack generation. (c) Beam with a crack of 10% of the beam thickness. (d) side view of the beam with a 10% crack.

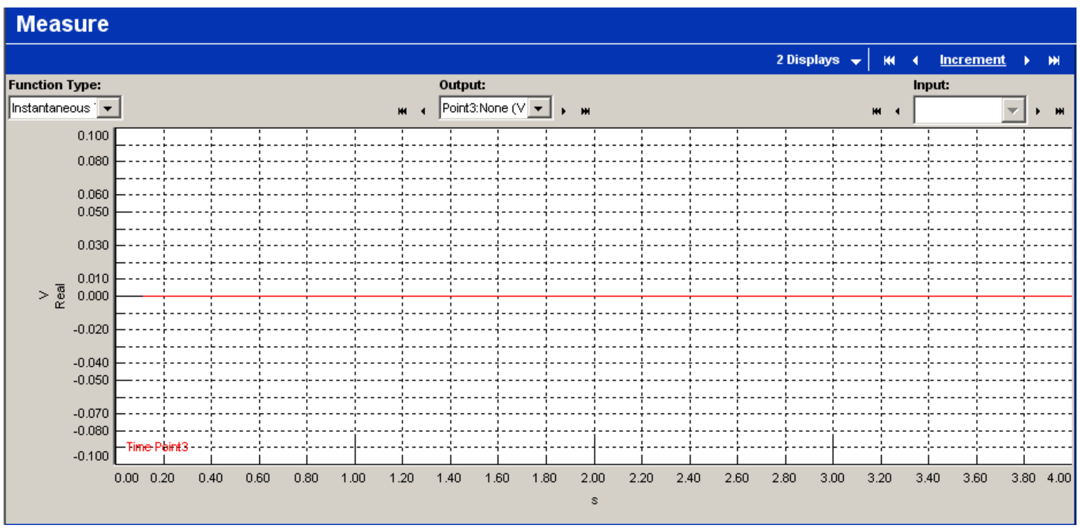

(a)

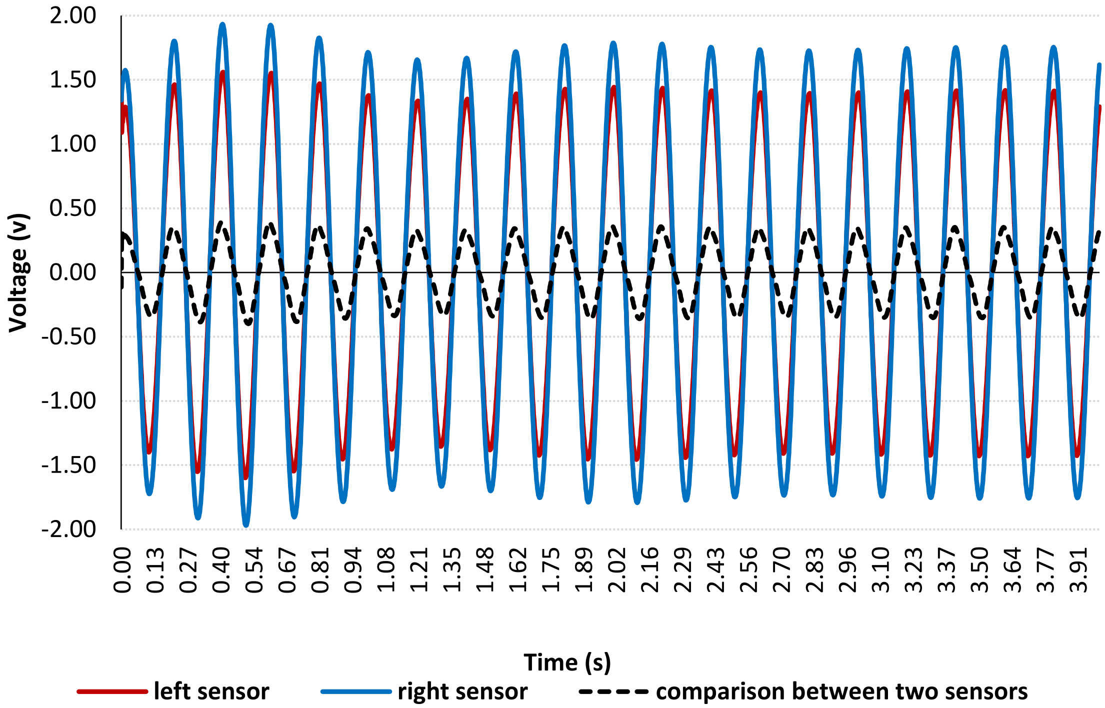

Voltage (v)
2.00
1.50
1.00
0.50
0.00
-0.50
-1.00
-1.50
-2.00
0.00
0.13
0.27
0.40
0.54
0.67
0.81
0.94
1.08
1.21
1.35
1.48
1.62
1.75
1.89
2.02
2.16
2.29
2.43
2.56
2.70
2.83
2.96
3.10
3.23
3.37
3.50
3.64
3.77
3.91
Time (s)
left sensor
right sensor
comparison between two sensors

(b)

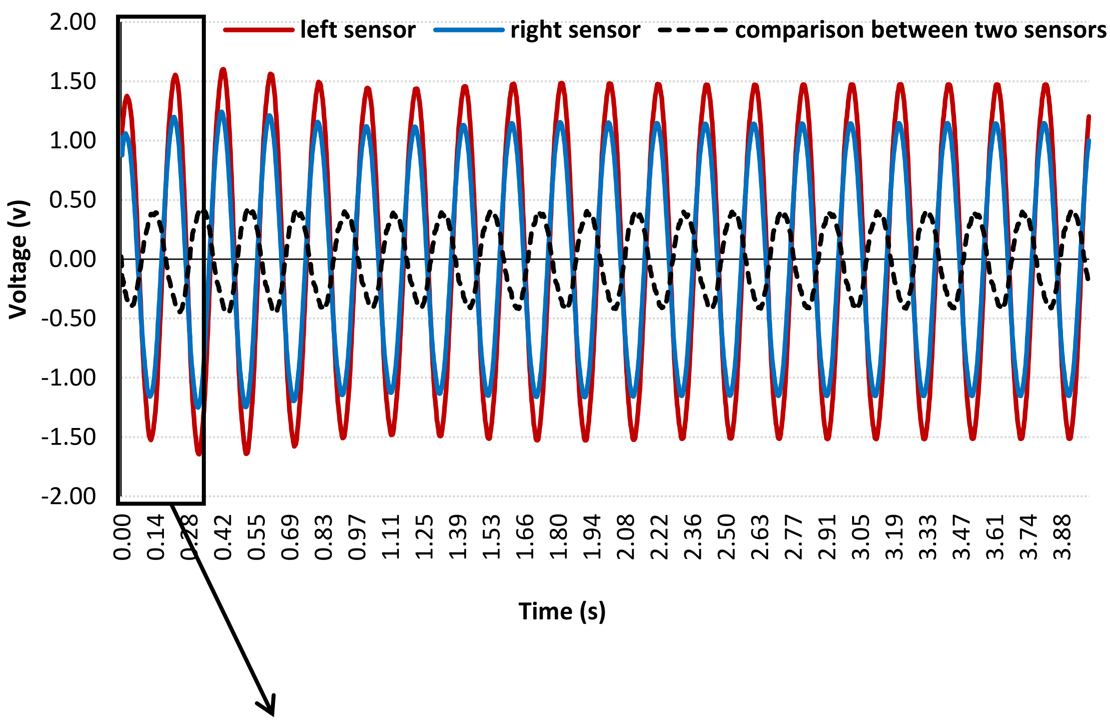

left sensor
right sensor
comparison between two sensors
Voltage (v)
2.00
1.50
1.00
0.50
0.00
-0.50
-1.00
-1.50
-2.00
0.00
0.14
0.28
0.42
0.55
0.69
0.83
0.97
1.11
1.25
1.39
1.53
1.66
1.80
1.94
2.08
2.22
2.36
2.50
2.63
2.77
2.91
3.05
3.19
3.33
3.47
3.61
3.74
3.88
Time (s)

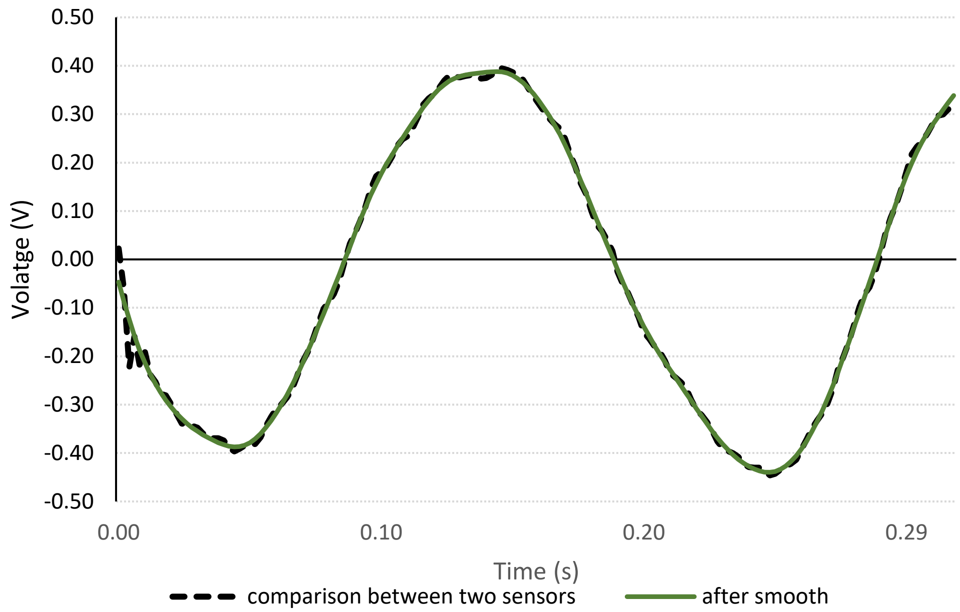

(c)

Figure 3-12. (a) Voltage signal of the beam with an intact coating from experimental vibration test. (b) The experimental voltage signal of the beam with a broken coating. (c) The experimental voltage signal of the beam with 10% crack beam with zoomed in filtered data by a smooth function. (All data are obtained under sinusoid excitation with the frequency of 5 Hz and amplitude of 0.0005 m for 4 s.)

After the experimental vibration test, voltage signals generated from the piezoelectric layers/patches are measured using WT SampEn in Matlab as the numerical simulations do. WT scale factor and repeat number are set as 5 and 6, respectively, based on the WT optimization from numerical studies. The SampEn variation ratio compared with the healthy beam with different base motion amplitudes are concluded in Table 3-4. Obvious noise in experimental studies is usually inevitable. Hence, a smooth function is needed to reduce the noise before entropy calculation in Matlab. The smooth function is a moving filter with the window size of 1% of the measured data length filtering high-frequency noise in the experimental data. After filtering the noise, I find that the entropy value of each piezo-layer becomes indistinguishable when I adjust the filter gradually. But the comparison signal between two piezo-layers is always sensitive to the existing of the open crack.

It is presented in Table 3-4 that for the case with base motion amplitude of 0.0005 m, the entropy variation ratio changes from 0 to 13% for the piezo-layer I when the crack initiates and increases to 10% of the beam thickness. And for the piezo-layer II, it changes from 0 to 3%. However, the entropy value calculated from the comparison between two piezo-layers increases from 0 to 567% along with the crack initiation and increasing to 10% of the beam thickness. This is induced by the strain singularity/concentration at the crack tip and clearly indicates the crack propagation. For the case with larger base motion amplitude of 0.001m, when the crack depth increases to 10% of the beam thickness from the initial stage, entropy variation ratio for the piezo-layer I drops a little to -1%. While the entropy variation ratios for the piezo-layer II and the comparison increase to 1587% and 748%, respectively, clearly indicating the crack severity increment. It is noted that the sensitivity for the crack strain concentration is higher with more obvious entropy value variation. The data from the piezo-layer II shows a low sensitivity with a small excitation (0.0005m), and when the excitation increases, which leads to a severer strain singularity at the crack, it becomes sensitive. However, for the comparison between two piezo-layers, it is sensitive even for the small excitation, and the entropy variation increases gradually when the excitation increases. These results are consistent with the entropy variation trend and findings in numerical studies. To confirm its reliability, I collect each vibration data 6 times and obtain the results by averaging.

Table 3-4. SampEn variation percentage compared with the healthy structure under experimental study

Base motion amplitude	**Crack depth (%)**	**Entropy variation compared with the healthy structure**		
		Piezo-layer I	**Piezo-layer II**	**Comparison between two layers**
0.5mm	**0**	0	0	0
	10	13%	3%	567%
1mm	**0**	0	0	0
	10	-1%	1587%	748%

In experimental studies, it is validated that the new smart coating and WT SampEn are feasible for the high sensitivity crack detection and notification of crack propagation. I can detect the damage at its initial stage by noticing the nonzero voltage between two piezoelectric patches, and then identify its propagation using WT SampEn measurement. Due to the limitation of experiment equipment, closed fatigue crack, considering both breathing and strain singularity effects is hard to prepare experimentally. However, as long as the breathing effect of closed cracks and strain singularity of open cracks can be identified individually, identification of a closed fatigue crack can be easily realized as revealed in numerical studies.

4. CRACK IDENTIFICATION WITH THE FREQUENCY COMPARISON FUNCTION (FCF) METHOD

4.1. Simulation Studies and Discussion

In this section, the simulation process obtaining the vibration signals is described briefly by referring section 3.1. Data analysis is then conducted in Matlab using FCF algorithm, and discussion based on the analysis results is processed afterward.

Figure 4-1 shows a schematic drawing of the beam mounted with piezoelectric patches, and the welding joint is emphasized in it. The major difference of the models between the study in section 2 and the current one is that the locations of two piezoelectric patches are on two sides of the welding joint for the current study. The geometric parameters of the beam and the piezoelectric layers are indicated in the figure. L is the length of the beam, l_p is length of the piezoelectric layer, H is the thickness of the beam and h_p is the thickness of the piezo-layer. The size and position of the weldment are also marked in the sketch.

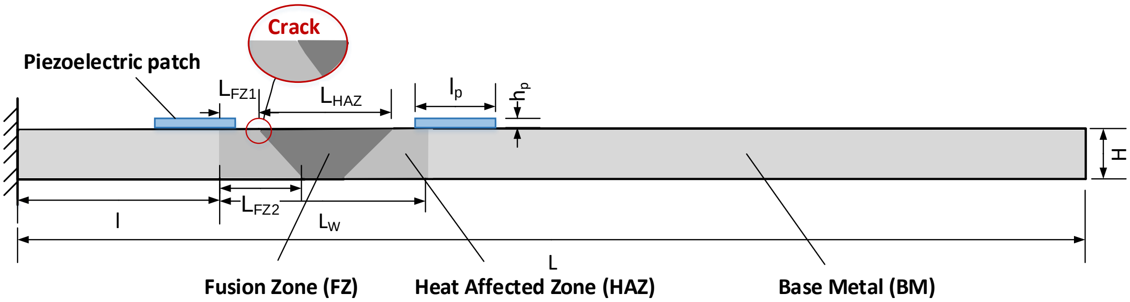

Figure 4-1. Welded cantilever beam with an open crack in the welding joint

According to the section 3, the welded beam mounted with the smart coating sensor is modeled in the FEM software ANSYS 19.2 as a plane model considering a crack crossing the beam width, and the parameters of the welded beam and the piezoelectric layers are shown in the table 4-1 as a case study (case 1).

Table 4-1. The geometric of the welded beam and the piezoelectric patches

Parameters	Welded beam (mm)	Piezoelectric patches (mm)
L	1000	-
$\mathbf{l_p}$	-	10
l	18	-
$\mathbf{L_w}$	16	-
$\mathbf{L_{HAZ}}$	12	-
$\mathbf{L_{FZ1}}$	2	-
$\mathbf{L_{FZ2}}$	7	-
W	20	-
$\mathbf{w_p}$	-	7
H	3	-
$\mathbf{h_p}$	-	0.5

Transient analysis is conducted afterward. External excitation is a sinusoidal base motion along the direction perpendicular to the beam (Y direction) at the fixed end (the end near the welding joint). And the frequency is set as 49 rad/s, while the first natural frequency of the beam is 52.59

rad/s from the modal analysis. The damping ratio is 1% during transient analysis. The time duration and interval for the transient analysis are defined as 5 s and 0.001 s respectively based on the convergence study done in section 3. Voltage data are collected from two piezoelectric patches indicating the simulated vibration signals, as shown in figure 4-2. Before using FCF, time-domain vibration signals are transformed into the frequency domain using FFT in Matlab to select the effective range for FCF calculation. Figure 4-3 displays the vibration signals from two piezo-layers in the frequency domain. And the effective frequency range for FCF calculation is set to be 40 Hz since distinct peaks occur in this frequency range as shown in Figure 4-3.

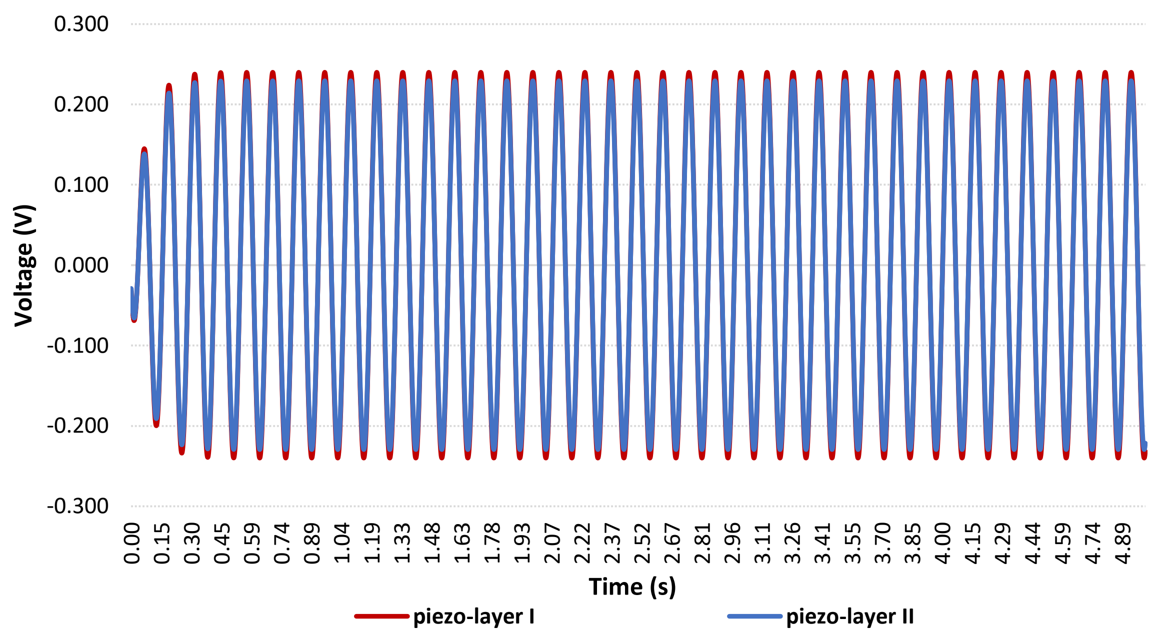

(a)

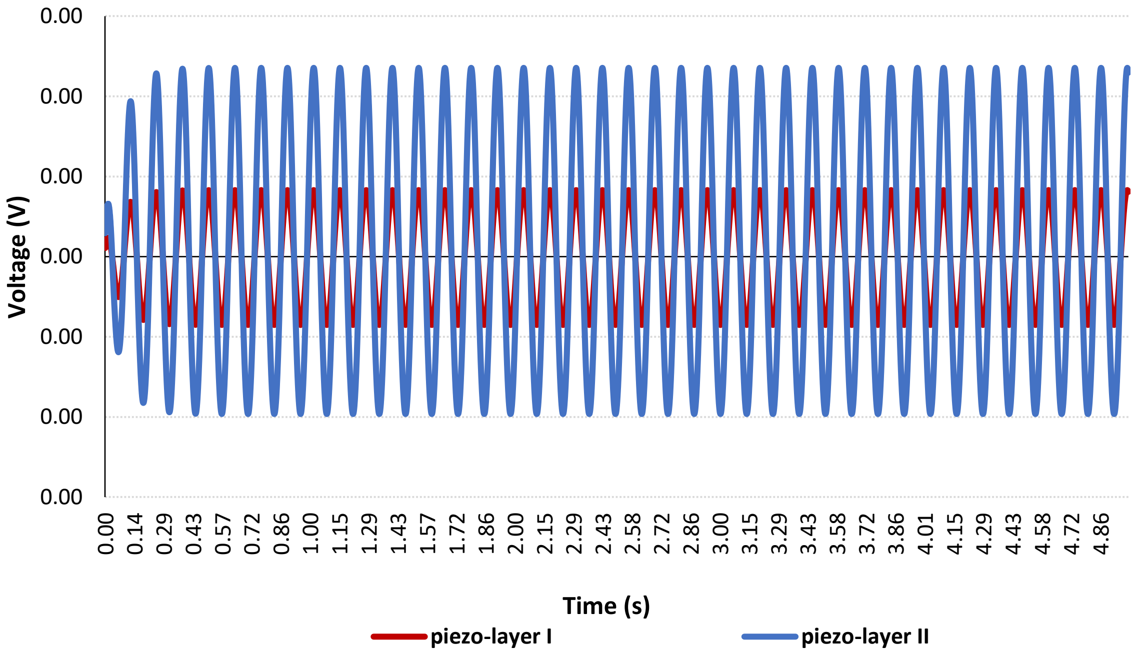

(b)

Figure 4-2. (a) Voltage signals generated from the simulation of a healthy beam (without the bridge coating broken); (b) Voltage signals generated from the simulation of the damaged beam with a crack of 25% of the beam thickness. Both beams are under harmonic base motion excitation with 0.005 m amplitude and 49 Rad/s frequency.

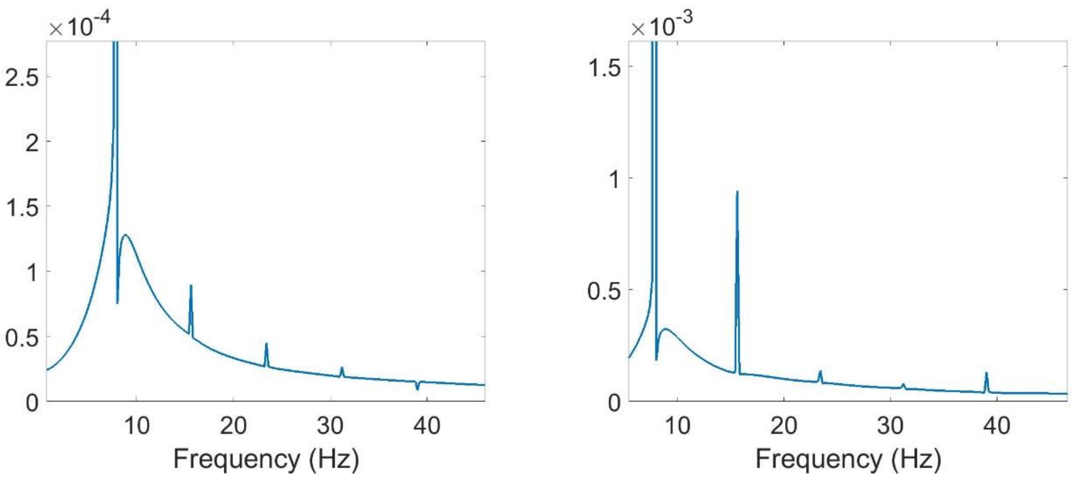

(a) (b)

Figure 4-3. (a) The zoom-in curve of the piezo-layer I frequency domain signal to focus on the peaks; (b) The zoom-in curve of the piezo-layer II frequency domain signal to focus on the peaks. A beam with a crack of 25% depth of the beam thickness under harmonic excitation of frequency of 49 rad/s and amplitude of 0.005 m is used as an example to show the data.

Simulated time-domain vibration signals are then calculated using the FCF algorithm in Matlab.

Compared to FRF, the signal generated from the piezoelectric patch near the fixed end of the beam (the piezo-layer I in this case) acts as the input signal, and the signal generated from the patch far from the fixed end (the piezo-layer II in this case) is the measured output signal of the local welding area. $H1_c(f)$ calculation is applied under this condition since the vibration signal of the piezo-layer II (output 2) is expected to be noisy compared to the vibration signal of the piezo-layer I (output 1), and I define,

$$H1_c(f) = \frac{Cross\ Spectral\ Density\ of\ the\ \ output\ 1\ and\ Output\ 2}{Spectral\ Density\ of\ the\ output\ 1}, \quad (4\text{-}1)$$

'pwelch' function in Matlab is used to calculate the spectral density in the frequency domain of the output 1, and 'cpsd' function in matlab is used to measure the cross-spectral density in the frequency domain of the output 1 and the output 2 (piezo-layer I signal and piezo-layer II signal, respectively).

To quantify the FCF result, standard deviation (stdev) value for the magnitude curve of the $H1_c(f)$ plot is calculated. Meanwhile, effective frequency range of the $H1_c(f)$ amplitude curve is decided as discussed before according to the output 1 and output 2 in the frequency domain.

In the study, the crack is identified from two aspects. One is the strain concentration level at the crack tip, and another is the crack depth. The vibration signals generated from the simulation are separated into three groups. Group 1 results are collected by changing the excitation amplitude. Group 2 and group 3 results are obtained by changing the crack depth of the beam model with the same excitation amplitude. For group 1, there is only one beam model, and the crack depth is 10% of the beam thickness. The base motion frequency is fixed as 49 rad/s, and the amplitude varies from 0.0015 m to 0.0055 m, then the strain concentration level at the crack tip increases from 0.000515 to 0.002834 accordingly. For group 2, the external excitation is fixed with a frequency of 49 rad/s and amplitude of 0.005 m, and the crack depth of the beam model changes from 3% to

40% of the beam thickness. For group 3, the external excitation is a set of random base motions with the amplitude range of no more than 0.0005 m, and the crack depth changes from 3% to 40% of the beam thickness. The meshing configuration for beam models with different crack depth is similar at the crack tip area and the rest part of the mounted beam models. The vibration signals of the healthy beam are also simulated as the reference data. The meshing configuration for the healthy beam model at the weldment is a little different from the cracked beam models since there is no refined meshing at the crack area. And the meshing of the rest part of the beam is the same with other damaged beam models. Besides, to better understand the damage detection feasibility under different excitation cases, another study under random excitation applied to the beam models with different crack depth is also conducted.

Figure 4-4 provides the variation trend of the stdev value in accordance with the variation of the strain concentration level at the crack tip for a welded beam with a breathing crack. The FCF stdev values show clear variation with strain concentration change and a high crack identification sensitivity. When the strain concentration level is at 0.00077, the FCF stdev value is only 0.0021, and the value gets larger along with the increasing strain concentration. The FCF stdev value increasing trend is sharp at the beginning of the strain concentration increment. When the crack tip strain changes from 0.00077 to 0.00103, the FCF stdev value rises from 0.0021 to 0.0886. This increasing trend becomes smoother when the strain concentration level reaches 0.00283. The increment of the crack tip strain from 0.00283 to 0.00309 leads to the variation of the FCF stdev from 0.2957 to 0.3089. To emphasis the sensitivity, the comparison ratio of the FCF stdev value between the damaged and healthy beams is shown on the right of the figure as the secondary axis. Since the stdev value for the healthy beam is close to 0 (0.001), the FCF stdev ratio comparing to it is very large and increases significantly along with the strain level increment. It reaches 30760% when the strain concentration level is at 0.00309.

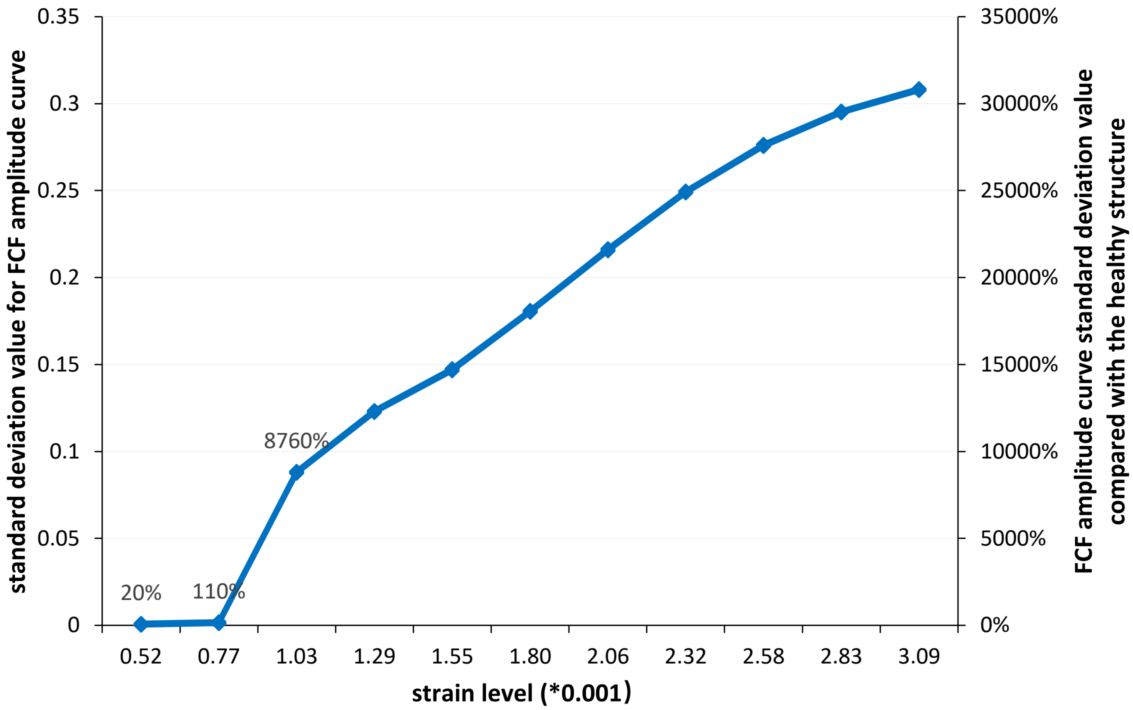

Figure 4-4. FCF stdev value for FCF amplitude curve versus different tip strain levels considering both crack breathing and material nonlinearity (closed breathing crack). The crack is 10% depth of the beam thickness with harmonic excitation of frequency of 49 rad/s and increasing excitation amplitude.

Figure 4-5 shows the variation trend of the FCF stdev value for simulation group 2. In group 2, the variable is the crack depth. When the crack is 3% depth of the beam thickness, the FCF stdev value is 0.0018, and the comparison ratio considering the healthy structure is not obvious at around 80%. The FCF stdev value increases along with the increment of the crack depth, and the increasing trend is smooth in the beginning then becomes sharper. When the crack depth is lower than 12% of the beam thickness, the increasing trend is stable, and the FCF stdev value reaches 0.3742, when the crack depth gets to 12%. When the crack is 15% of the beam thickness, the stdev value is 0.7563, and it increases to 11.2725 when the crack depth reaches 40% of the beam thickness. Observed from the FCF stdev comparison ratio with the health case, the value is as high as 2710%

when the crack propagates to 5%. It shows a high sensitivity for crack detection at the initial stage. And when the crack reaches 40% of the beam thickness, the ratio increases to 1127150%.

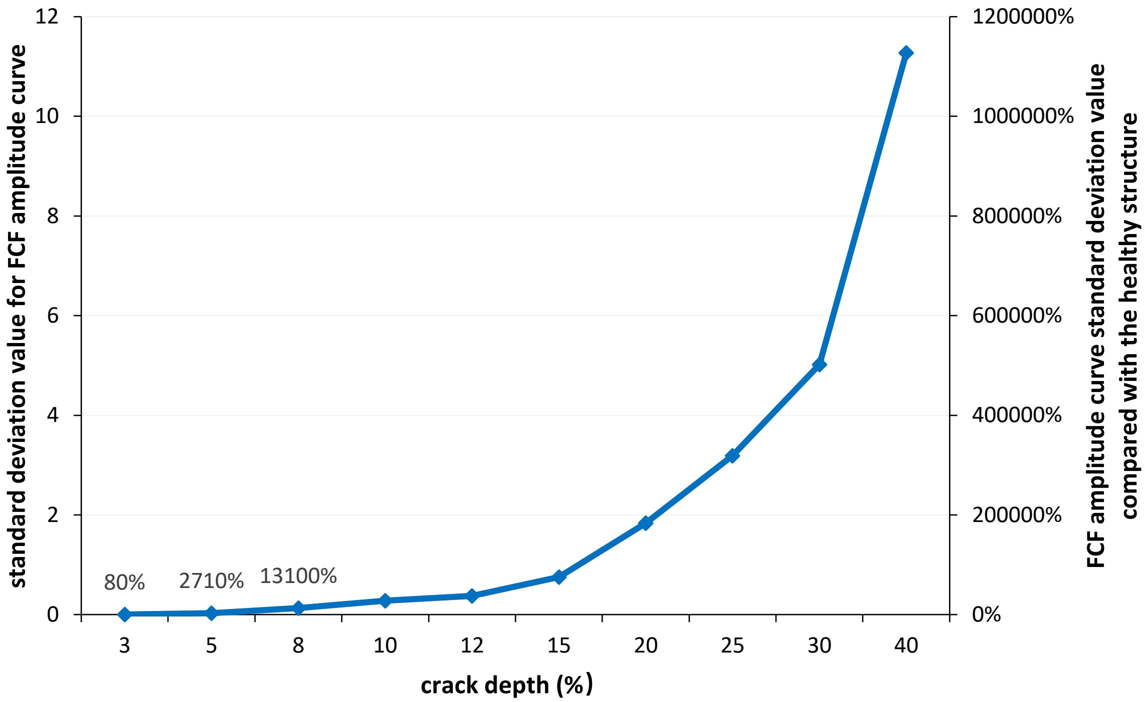

Figure 4-5. FCF stdev value for FCF amplitude curve versus different crack depth under the same harmonic excitation considering both crack breathing and material nonlinearity. Base motion amplitude and frequency are 0.005 m and 49 rad/s, respectively.

Figure 4-6 concludes the stdev variation trend for group 3. The beam models are the same with the group 2 with a random base motion excitation. It is seen from the figure 4-6 that the FCF stdev value variation trend is similar with the condition of the harmonic excitation. When the crack depth increases from 3% to 12%, the stdev value reaches 2.9513. Similar to the figure 4-5. The increasing trend becomes sharper and sharper afterwards, when the crack enlarges to 40% of the beam thickness, the stdev value becomes 18.4393, and the comparison ratio to the healthy beam is 1843830%.

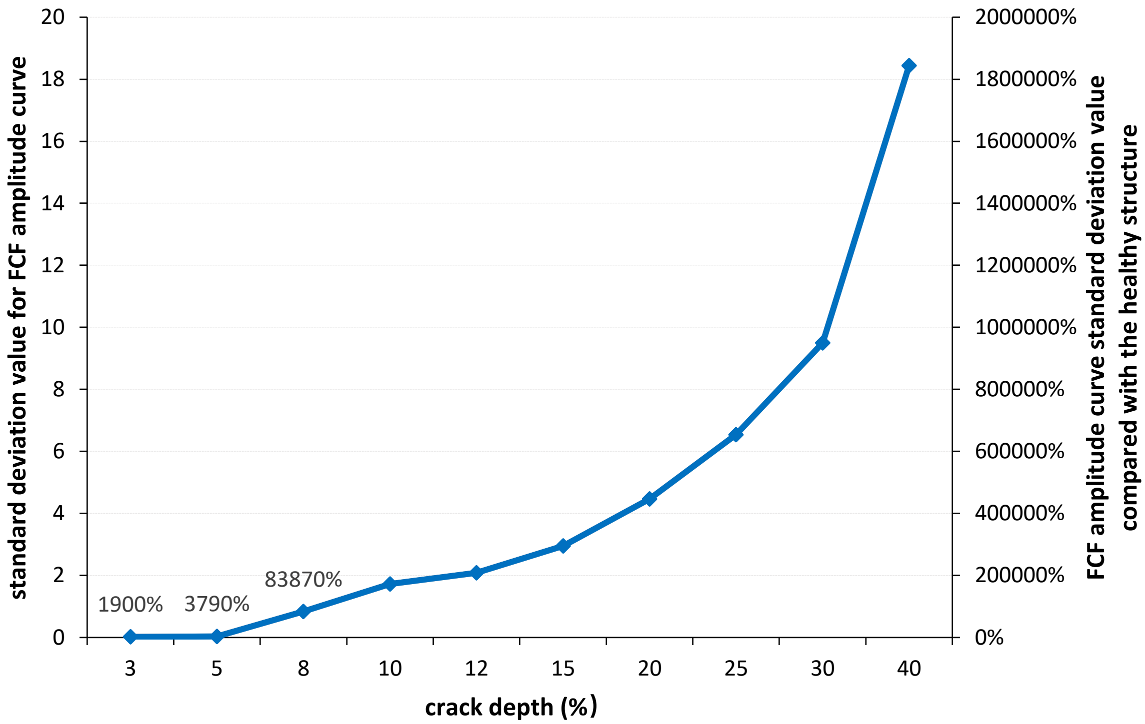

Figure 4-6. FCF stdev value for FCF amplitude curve versus different crack depth under random excitation considering both crack breathing and nonlinearity. Base motion amplitudes are totally random following white noise distribution in frequency domain with a variation range of ±0.0005 m.

To sum up, the FCF method is an effective way to evaluate the breathing crack with high sensitivity. And the increasing trend of the FCF stdev value showing in the curves considering the increment of the strain concentration level and the crack depth are quite steady and distinguishable. Meanwhile, crack detection and evaluation under random excitations are feasible and also with a high sensitivity using FCF measurement. Furthermore, FCF method is so much faster compared to the WT entropy measurement (section 3) due to the simple algorithm without any auxiliary pre-data-processing functions. The overall FCF running time is only around 0.03 s considering the 5 s vibration signal in simulation studies (2.71 GHz, 8GB RAM). On the other hand, the running time for the entropy method is 156 s with the wavelet transformation as pre-data processing. Thus, real-time damage identification is realized by FCF.

Simulation studies are conducted on other two different welded beam structures with the welding joint and crack located at different positions in order to test the universality of the FCF method. Different from case 1 as discussed before, the position of the welding joint for case 2 is 0.04 m away from the fixed end, and for case 3, the position of the welding joint is 0.22 m away from the fixed end. FEM simulations under ANSYS APDL for the additional cases are the same as case 1. The damaged beam models are with 10% (of the beam thickness) closed crack. Harmonic base motion excitations are applied on the beam models with the frequency of 49 rad/s. To be consistent with the strain level in the crack tip in case 1, the base motion amplitudes are set as 0.0012 m to 0.006 m for case 2, with the strain level in the crack tip increasing from 0.000502 to 0.00251. Meanwhile, the base motion amplitudes for case 3 are set as 0.004 m to 0.018 m, accordingly, with the strain level varying from 0.00055 to 0.00249.

The FCF stdev variation trends for the three different cases are organized in figure 4-7. The variation trend for three cases are quite similar with sharp initial increment. When the strain level at the crack tip reaches a certain value (around 0.0015), the FCF stdev value becomes steady. For the case 2, the FCF stdev value is only 0.0011 when the strain concentration level at the crack tip is 0.0005. When the strain concentration changes from 0.0005 to 0.0021, the stdev value increases from 0.0011 to 0.1504. This increasing trend becomes smoother afterwards. The strain increment from 0.0021 to 0.00251 leads to the variation of the FCF stdev value from 0.1504 to 0.1656. For the case 3, the FCF stdev value is 0.0098 when the initial strain concentration level is 0.00055. When the strain concentration increases from 0.00055 to 0.0018, the stdev value increases from 0.0098 to 0.1427. Then the variation trend becomes smooth. The FCF stdev value changes from 0.1427 to 0.1557 when the strain concentration level at the crack tip increases from 0.0018 to 0.00249. It is concluded from these results that when the welding joint is becoming far away from the fixed end, the variation range for the FCF stdev value is slightly narrow down. However, these values are quite close to each other for different beam structures considering same strain concentration level.

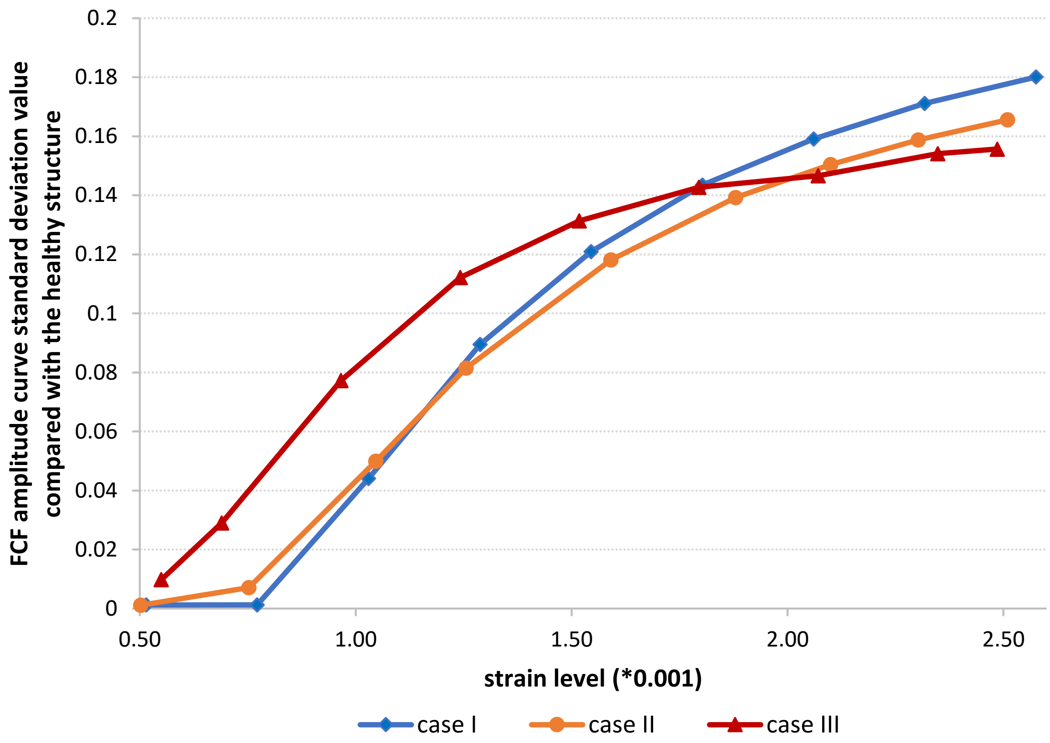

Figure 4-7. Comparison between different cases with crack located at different position on the tested beam considering the standard deviation value for FCF amplitude curve versus different tip strain levels. The crack is closed at rest of the beam and with 10% depth of the beam thickness with harmonic excitation of frequency of 49 rad/s and increasing excitation amplitude.

4.2. Experimental Validation and Discussion

In this section, experimental studies are conducted to validate the simulation results on crack identification with the FCF measurement. To set up the experiment, three aluminum alloy beams are mounted together without any gap to simulate the damaged beam with a closed crack. Prime et al. [83] and Douka et al. [84] have used this technique as well to simulate breathing cracks during experiments.

In the current experiment, three beams are prepared, one is the healthy beam, and the other two are cracked beams with 25% depth crack and 50% depth crack, respectively. The crack is located at 0.01 m from the fixed end of the cantilever beam for the cracked beam. The overall beam span is 2 m. However, the fixed point is in the center and makes the effective span as 1 m, which is consistent with the simulation model. The healthy beam (0%) is constructed by bonding two equivalent beams referring to Prime et al. [38] to narrow down the differences between the healthy beam and the cracked beams to the crack region. The overall thickness of each beam is 6.36 mm, and the width is 20 mm.

Figure 4-8 shows the experimental setup of the beam mounted with the smart coating sketched in figure 3-1. The length of the piezoelectric patches is the same with the simulations, the width and the thickness are 7 mm and 0.5 mm, respectively. The aluminium beam is attached to a shaker provided by the Modal Shop Inc. (Model 2100E11 100lbf Modal Shaker) in the fixed point. During the experiment, two kinds of excitation are applied to the beam. One is harmonic base motion, which is provided by the shaker, the frequency is 5 Hz (close to the first natural frequency of the beam), and the amplitude is around 0.0005 m. Another is a set of random base motion (white noise) excited by the shaker with an amplitude range of no more than 0.0005m, this random excitation signal is generated by the same LMS SCADAS Mobile (type SCM05) data acquisition system as the experiment study in chapter 3.2. Figure 4-9 shows the damaged beam with 25% depth crack and 50% depth crack with amplified details at the coating. Figure 4-9 (a) and (c) display the top view and side view of the cracked beam with 50% crack, respectively, and figure 4-9 (b) and (d) show the damaged beam with 25% crack. Two piezoelectric layers of the coating are connected to the LMS data acquisition system. To reduce the inevitable environmental noise effect on the testing results, I did the test 5 times for each different types of excitations taking the average stdev as discussed below.

Figure 4-8. Overview of the whole experiment set up. (The beam is under base motion from the shaker supporting the whole structure at the center)

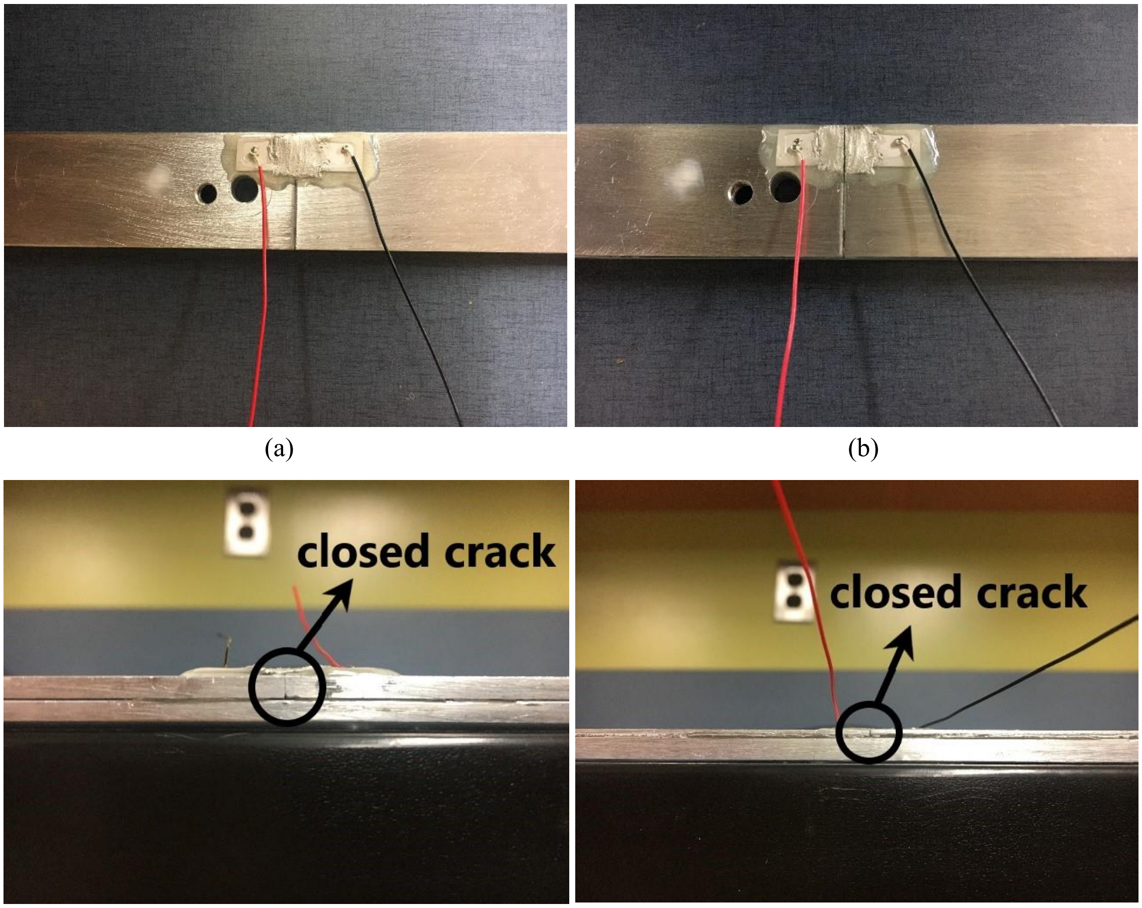

(c) (d)

Figure 4-9. (a) Overview Installation of the smart coating (beam with the intact coating). (b) Beam with the broken coating which indicate the beginning of the crack generation. (c) Side view of the beam with a crack of 50% of the beam thickness. (d) Side view of the beam with a 25% crack.

Voltages of the piezo-layers read from the LMS are then measured in Matlab using FCF algorithm. Here, I classify the signals into two groups based on different excitations (harmonic or random). FCF stdev values for group 1 with harmonic base motion are shown in table 4-2. The FCF stdev value increases from 0.0367 to 0.0696 when the crack happens to the beam and increases to 25% depth of the beam thickness. When the crack propagates and reaches 50% depth of the beam thickness, the FCF stdev value increases to 0.1945. If shown in the comparison ratio between the damaged beam and the healthy beam, the value changes from 0 to 89.64% when the crack becomes 25% depth of the beam thickness and goes up to 429.97% when the crack depth reaches 50%. Table 4-3 shows the results from the test group 2 with random excitation. The FCF stdev value for the healthy beam is used as a reference as well. When the crack initiates and increases to 25% of the beam thickness, the FCF stdev value is 0.0547, and the increasing ratio compared to the healthy beam is 49.05%. Afterward, the FCF stdev value reaches 0.1013, and the comparison ratio increases to 175.75%, when the crack depth rises to 50% of the beam thickness.

Table 4-2. Experimental FCF stdev value of the FCF amplitude curve and its variation percentage compared with the healthy structure under harmonic base motion (Frequency of 5 Hz and amplitude of 0.0005 m)

Crack depth	The FCF amplitude curve stdev	Percentage to the healthy beam
0	0.0367	0
25%	0.0696	89.64%
50%	0.1945	429.97%

Table 4-3. Experimental FCF stdev value of the FCF amplitude curve and its variation percentage compared with the healthy structure under random excitation

Crack depth	The FCF amplitude curve stdev	Percentage to the healthy beam
0	0.0367	0
25%	0.0547	49.05%
50%	0.1012	175.75%

It should be noted that the experimental testing set up and structures are not the same as the simulation one. Meanwhile, the inevitable environmental and sensor noises in the experiment also affect the tests leading to different results. And for the random excitation experiments, it is hard to control the base motion amplitude. To avoid the damage of the tested structure with the glued sensor, I used small random excitations with the amplitude variation range of ±0.0005 m. So, the experimental setup and obtained values cannot precisely match the simulation ones. Due to the different working environments and the noises, the FCF stdev value for the healthy beam is larger in the experiment. Hence the experimental results for FCF stdev variation with crack are not so obvious as shown in simulations. However, it still shows excellent sensitivity considering crack detection and evaluation under harmonic and random excitation from the experiments. Through the physical test, it is hence confirmed the efficiency of FCF algorithm applied without auxiliary of signal smooth functions or amplified functions.

5. Conclusions and Future Work

In this thesis, two crack identification methods, WT SampEn and FRF, are studied. Both methods are applied with the new smart coating sensor to detect and evaluate the crack of a welded beam. The new piezoelectric sensor is composed of double/three piezoelectric elements, a conductive layer, and an insulator. It acts as both the sensor to identify the crack and the energy harvester during vibrating. The sensor can be easily applied to rough engineering surfaces as well. During the study, FEA models are established to simulate beam vibration and the generated signals from the piezoelectric coating, considering both crack breathing and material nonlinearity at the crack. And then both methods are introduced to estimate the weak crack-induced perturbations hidden in the dynamic signal. Experimental studies are subsequently conducted, showing a good consistency conclusion compared with simulation results.

5.1. The WT SampEn measurement

(1) By comparing the dynamics signals on two sides of a crack so as to study and analyze the local strain concentration effect on structural dynamic responses, entropy measurement can realize the identification of an open crack with the decent sensitivity and steady entropy increasing trend considering the increment of the local strain concentration.

(2) The entropy variation ratio increases obviously corresponding to the increment of the strain level at the crack tip and reaches a limit at a certain strain value considering both crack breathing and material nonlinearity. It shows higher sensitivity when only considering the

crack breathing because of the much lower entropy value calculated with the optimized algorithm for the healthy state beam.

(3) The entropy variation ratio shows a sharp increment trend in the crack depth range between 5% and 10%. It presents that the proposed crack identification method possesses a high sensitivity for crack identification even at very early stages of the crack with the depth of 5% of the beam thickness.

(4) Experimental testing for the intact beam and the beam with broken coating shows the smart coating is capable of detection of initial cracks. And further testing for 10% open cracked beam shows a high sensitivity of the crack severity increment estimating capability considering the strain concentration at the crack tip based on the comparison vibration signal between two piezoelectric layers.

5.2. The FCF method

(1) The FCF methodology is sensitive to identify the breathing cracks (closed at the beam rest position), and it can notice the initiation of a crack with the depth as small as 3% of the beam thickness.

(2) By conducting simulations to the beam-type structure with the crack at different locations of the beam, I conclude that the FCF method can realize the crack severity evaluation for beams with the crack at different locations.

(3) Based on the simulation and experimental studies, the FCF method possesses two major advantages. First, FCF can be applied without employing pre-data-processing functions to smooth or amplify the vibration signals. Thus, the real-time damage identification can be

realized accordingly. Secondly, FCF is a sensitive and effective method to detect closed cracks under random excitation, which is a more general practical working condition.

5.3. Future work

Since there are still limitations for the WT SampEn and the FCF methods, the first expectation of the future work will be finding a way to realize the fast real-time open crack detection with WT SampEn method. In addition, to address the problem of being insensitive to the strain singularity for the FCF method is an alternative solution of real time open crack detection. By this way, both methods can be applied to build a comprehensive system for crack evaluation. Hopefully, the whole crack identification system can be applied to practical engineering fields soon.

Furthermore, the exact quantification of crack severity in different structures, such as plates and shells, will also be one of the important future work with the proposed smart coating sensor. A proper signal filter should be designed to further reduce the environmental noise in the numerical and experimental studies. This will be a great breakthrough for crack detection and can be used as a quantification standard for different practical working conditions.

REFERENCES

[1] Hong X B, Liu Y, Lin X H, Luo Z Q and He Z W 2018 Nonlinear ultrasonic detection Method for delamination damage of lined anti-corrosion pipes using PZT transducers *Applied Sciences* **8(11)**

[2] Ronald O'Brien, Juan F, Nicolás P and Leonardo M 2017 A pattern recognition system based on acoustic signals for fault detection on composite materials *European Journal of Mechanics A/Solids* **64** 1-10

[3] Mohammadhadi S, Maha G, Dagmar S and Douglas T 2017 On acoustic emission for damage detection and failure prediction in fiber reinforced polymer rods using pattern recognition analysis *Smart Materials and Structures* **26(6)** 065023

[4] Sathish S, Welter J, Jata K, Schehl N and Boehnlein T 2012 Development of nondestructive non-contact acousto-thermal evaluation technique for damage detection in materials *Review of Scientific Instruments* **83(9)** 095103/1-095103/11

[5] Yu X and Fu X 2015 The prototype of fatigue damage detection by the method of Metal Magnetic Memory Testing. In Mechatronics Engineering and Electrical Engineering *Proceedings of the 2014 International Conference on Mechatronics Engineering and Electrical Engineering, CMEEE 2014* 115–117 CRC Press/Balkema

[6] Huang Z C, Qin Z Y and Chu F L 2014 A review about vibration problems of thin-walled structures with viscoelastic damping layer *Journal of Vibration and Shock* **33** 105-113

[7] Shokri T, Nemati N and Nanni A 2012 Acoustic emission noise assessment of loaded members in laboratory and field environments *In Proceedings of SPIE - The International Society for Optical Engineering* **8347** 83471T

[8] Safaa Kh. Al-Jumaili, Matthew R. Pearson, Karen M. Holford, Mark J. Eaton, Rhys Pullin 2016 Acoustic emission source location in complex structures using full automatic delta T mapping technique *Mechanical Systems and Signal Processing* **72–73** 513-524

[9] Doebling S W, Farrar C R and Prime M B 1998 A summary review of vibration-based damage identification methods *The Shock and Vibration Digest* **30** 91–105.

[10] Yan Y J, Cheng L, Wu Z Y and Yam L H 2007 Development in vibration-based structural damage detection technique *Mechanical Systems and Signal Processing* **21 (5)** 2198-2211

[11] Fan W and Qiao P Z 2010 Vibration-based Damage Identification Methods: A Review and Comparative Study *Structural Health Monitoring* **10 (1)** 83-111

[12] Das S, Saha P and Patro S K 2016 Vibration-based damage detection techniques used for health monitoring of structures: a review *Journal of Civil Structural Health Monitoring* **6 (3)** 477–507

[13] Islam A S and Craig K C 1994 Damage detection in composite structures using piezoelectric materials (and neural net) *Smart Materials and Structures* **3 (3)** 318

[14] Hadjigeorgiou E P, Stavroulakis G E and Massalas C V 2006 Shape control and damage identification of beams using piezoelectric actuation and genetic optimization *International Journal of Engineering Science* **44 (7)** 409-421

[15] Jiang L J, Tang J and Wang K W 2008 On the tuning of variable piezoelectric transducer circuitry network for structural damage identification *Journal of Sound and Vibration* **309 (3)** 695-717

[16] Zhao S, Wu N and Wang Q 2016 Crack identification through scan-tuning of vibration characteristics using piezoelectric materials *Smart Materials and Structures* **26** 025005
[17] Zhao S, Wu N and Wang Q 2016 Damage detection of beams by a vibration characteristics tuning technique through an optimal design of piezoelectric *International Journal of Structural Stability and Dynamics* **16 (10)** 1550070
[18] Wu N, Osho S, Faisal F and Zhao S 2016 Crack detection with self-powered wireless smart coating sensor *Proceedings The NDT Conference in Canada*
[19] Dessi D, Camerlengo G 2015 Damage identification techniques via modal curvature analysis: overview and comparison *Mechanical Systems and Signal Processing* **52–53** 181–205
[20] Yan G, De Stefano A, Matta E and Feng R 2013 A novel approach to detecting breathing-fatigue cracks based on dynamic characteristics *Journal of Sound and Vibration* **332** 407–422
[21] Whalen T M 2008 The behavior of higher order mode shape derivatives in damaged, beam-like structures *J Sound Vib* **309** 426-464
[22] Chen L J and Yu L 2013 Structural nonlinear damage identification algorithm based on time series ARMA/GARCH model *Adv Struct Eng* **16(9)** 1597-1609
[23] Wang Y, Liang M and Xiang J 2014 Damage detection method for wind turbine blades based on dynamics analysis and mode shape difference curvature information *Mechanical Systems and Signal Processing* **48(1-2)** 351-367
[24] Yang Z B, Radzienski M, Kudela P and Ostachowicz W 2017 Fourier spectral-based modal curvature analysis and its application to damage detection in beams *Mechanical Systems and Signal Processing* **84** 763-781
[25] Pandey A K, Biswas M and Samman M M 1991 Damage detection from changes in curvature mode shapes *J Sound Vib* **145** 321-332
[26] Cawley P and Adams R D 1979 The location of defects in structures from measurements of natural frequencies *J Strain Anal* **14(2)** 49-57
[27] Cha Y and Buyukozturk O 2014 Modal strain energy based damage detection using multi-objective optimization *Structural Health Monitoring* **5** 125-133
[28] Modena C, Sonda D and Zonta D 1999 Damage localization in reinforced concrete structures by using damping measurements, damage assessment of structures *The International Conference on Damage Assessment of Structures (DAMAS '99)* 132–141 Dublin, Ireland
[29] Muscolino G and Santoro R 2017 Explicit Frequency Response Function of beams with Crack of Uncertain Depth *Procedia Engineering* **199** 1128-1133
[30] Wang J, Wang C and Zhao J 2017 Frequency response function-based model updating using Kriging model *Mechanical Systems and Signal Processing* **87**(PA) 218-228
[31] Su W C, Huang C S, Hung S L, Chen L J and Lin WJ 2012 Locating damaged storeys in a shear building based on its sub-structural natural frequencies *Eng Struct* **39** 126-138
[32] Huang Q, Xu Y L, Li J C, Su Z Q and Liu H J 2012 Structural damage detection of controlled building structures using frequency response functions *J Sound Vib* **331** 3476-3492
[33] da Silva S, Dias J M, Lopes J V and Brennan M J 2008 Structural damage detection by fuzzy clustering *Mechanical Systems and Signal Processing* **22(7)** 1636-1649
[34] Hwang H Y, Kim C 2004 Damage detection in structures using a few frequency response measurements *J Sound Vib* **270** 1-14
[35] Askegaard V and Mossing P 1988 Long-term observation of RC-bridge using changes in natrual frequencies *Nordic Concr Res* **7** 20-27
[36] Yu L, Zhu J H and Yu L L 2013 Structural damage detection in a truss bridge model using

fuzzy clustering and measured FRF data reducing by principal component projection *Adv Struct Eng* **16(1)** 207-217
[37] Chen J and Garba J A 1988 On-orbit damage assessment for large space structures AIAA J **26(9)** 1119-1126
[38] Li H, Hyang Y, Ou J and Bao Y 2011 Fractal dimension based damage detection method for beams with a uniform cross-section Comput Aided Civil Infrastruct Eng **26(3)** 190-206
[39] Wang J and Qiao P 2007 Improved damage detection of beam type structures using uniform load surface Struct Health Monit **6(2)** 99-110
[40] Fan W and Qiao P 2011 Vibration-based damage identification method: a review and comparative study *Struct Health Monit* **10(1)** 83-111
[41] Wang S 2013 Damage detection in offshore platform structures from limited modal data *Appl Ocean Res* **41** 48-56
[42] Shi Z Y, Law S S and Zhang L M 1998 Structural damage localization from Modal strain energy change J Sound Vib **218(5)** 825-844
[43] Cornwell P 1999 Application of the strain energy damage detection method to plate-like structures *J Sound Vib* **224(2)** 359-374
[44] Wang S Q and Li H J 2012 Assessment of structural damage using natural frequency changes *Acta Mechanica Sinica* **28** 118-27
[45] Yang Z B, Radzienski M, Kudela P and Ostachowicz W 2017 Fourier spectral-based modal curvature analysis and its application to damage detection in beams *Mechanical Systems and Signal Processing* **84** 763-781
[46] Moughty J J and Casas J R 2017 A State of the Art Review of Modal-Based Damage Detection in Bridges: Development, Challenges, and Solutions *Applied Sciences* **7 (5)** 510
[47] Kim H and Melhem H 2004 Damage detection of structures by wavelet analysis *Engineering Structures* **26 (3)** 347-362
[48] Wu N and Wang Q 2011 Experimental studies on damage detection of beam structures with wavelet transform *International Journal of Engineering Science* **49 (3)** 253-261
[49] Ghanbari A, Wu N and Wu C 2018 Experimental study on the crack detection with optimized spatial wavelet analysis and windowing *Mechanical Systems and Signal Processing* **104** 619-630
[50] Wimarshana B, Wu N and Wu C 2017 Crack identification with parametric optimization of entropy & wavelet transformation *Structural Monitoring and Maintenance* **4 (1)** 33-52
[51] Wimarshana B, Wu N and Wu C 2017 Application of entropy in identification of breathing cracks in a beam structure: Simulations and experimental studies *Structural Health Monitoring* doi:1475921717704626
[52] Boltzmann L 1877 Ueber die Beziehung eines allgemeine mechanischen Satzes zum zweiten Hauptsatzes der Warmetheorie *Sitzungsber. Akad. Wiss. Wien, Math.-Naturwiss. Kl.* **75** 67-73
[53] Shannon C E 1948 A mathematical theory of communication *Bell System Technical Journal* **27** 379-423, 623-56
[54] Kolmogorov A N 1958 New metric invariant of transitive dynamical systems and endomorphisms of lebesgue spaces *Doklady of Russian Academy of Sciences* **119 (5)** 861–864
[55] Kolmogorov A N 1959 Entropy per unit time as a metric invariant of automorphism *Doklady of Russian Academy of Sciences* **124** 754–755
[56] Sinai Y G 1959 On the notion of entropy of a dynamical system *Doklady of Russian Academy of Sciences* **124** 768–771

[57] Diambra L, De Figueiredo J and Malta C P 1999 Epileptic activity recognition in EEG recording *Physica A: Statistical Mechanics and its Applications* **273** 495–505
[58] Richman J S and Moorman J R 2000 Physiological time-series analysis using approximate entropy and sample entropy *American Journal of Physiology-Heart and Circulatory Physiology* **278 (6)** H2039–H2049
[59] Leverick G, Szturm T and Wu C Q 2014 Using entropy measures to characterize human locomotion *Journal of Biomechanical Engineering* **136 (12)** 121002-121002-8
[60] Ducksbury P G 2000 Target detection and intelligent image compression *Proceedings SPIE-AeroSense* pp. 86–97
[61] Ducksbury P G and Varga M J 2001 Feature detection and fusion for intelligent compression. *Proceedings SPIE- Aerospace/defense sensing, simulation, and controls* pp. 162–173
[62] Pincus S and Kalman R E 2004 Irregularity, volatility, risk, and financial market time series *Proceedings of the National academy of sciences of the United States of America* **101** 13709–13714
[63] Pincus S M 1991 Approximate entropy as a measure of system complexity *Proceedings of the National Academy of Sciences of the United States of America* **88 (6)** 2297-2301
[64] An Y H and Ou J P 2013 Structural damage localisation for a frame structure from changes in curvature of approximate entropy feature vectors *Nondestructive Testing and Evaluation* **29 (1)** 80-97
[65] Costa M, Goldberger A L and Peng C K 2002 Multiscale entropy analysis of complex physiologic time series *Physical Review Letter* **89** 068102
[66] Costa M, Goldberger A L and Peng C K 2005 Multiscale entropy analysis of biological signals *Physical Review E* **71** 021906
[67] Liu H and Han M 2014 A fault diagnosis method based on local mean decomposition and multi-scale entropy for roller bearings *Mechanism and Machine Theory* **75** 67-78
[68] Yan R, Liu Y and Gao R X 2012 Permutation entropy: A nonlinear statistical measure for status characterization of rotary machines *Mechanical Systems and Signal Processing* **29** 474-484
[69] Wu S, Wu P, Wu C, et al. 2012 Bearing fault diagnosis based on multiscale permutation entropy and support vector machine *Entropy* **14** 1343–1356
[70] Yang Z, Chen X, Jiang Y, et al. 2013 Generalized local entropy analysis for crack detection in beam-like structures *Nondestructive Testing and Evaluation* **29** 133–153
[71] Ren W and Sun Z 2008 Structural damage identification by using wavelet entropy *Engineering Structures* **30 (10)** 2840–2849
[72] Chang C C and Chen L W 2003 Vibration damage detection of a Timoshenko beam by spatial wavelet based approach *Applied Acoustics* **64** 1217–1240
[73] Kim H and Melhem H 2004 Damage detection of structures by wavelet analysis *Engineering Structures* **26** 347–362
[74] Rucka M and Wilde K 2006 Application of continuous wavelet transform in vibration based damage detection method for beams and plates *Journal of Sound and Vibration* **297** 536–550.
[75] Zhong S and Olutunde O S 2007 Crack detection in simply supported beams without baseline modal parameters by stationary wavelet transform *Mechanical Systems and Signal Processing* **21** 1853–1884
[76] Umesha P K, Ravichandran R and Sivasubramanian K 2009 Crack detection and quantification in beams using wavelets *Computer-Aided Civil and Infrastructure Engineering* **24** 593–607

[77] Newland D E 1994 Wavelet analysis of vibration. Part 1: theory *Journal of Vibration Acoustics* **116** 409–416
[78] Hou Z, Noori M and Amand R S 2000 Wavelet-based approach for structural damage detection *Journal of Engineering Mechanics* **126** 677–683
[79] Wang Q and Deng X 1999 Damage detection with spatial *wavelets International Journal of Solids and Structures* **36** 3443–3468
[80] Lam H F, Lee Y Y, Sun H Y, Cheng G F and Guo X 2005 Application of the spatial wavelet transform and Bayesian approach to the crack detection of a partially obstructed beam *Thin-Walled Structures* **43** 1–21
[81] Abbate A, DeCusatis C M and Das P K 2002 Wavelets and Subbands: Fundamentals and Applications Birkhauser, *Boston*, Massachusetts, USA
[82] James Wren 2009 A simple frequency response function *Progsig Noise & Vibration Blog* http://blog.prosig.com/2009/10/19/a-simple-frequency-response-function/
[83] Tamrin Tanha 2016 Finite element modeling of arc welded joint based on the experimental studies of the weldment *University of Manitoba*
[84] Tamarin Y 2002 Atlas of Stress-Strain Curves (Ohio: ASM International)
[85] Prime M B and Shevitz B W 1996 Linear and nonlinear methods for detecting cracks in beams *Proceedings of 14th International modal analysis conference* Michigan February
[86] Douka E and Hadjileontiadis L J 2005) Time-frequency analysis of the free vibration response of a beam with a breathing crack *NDT & E International* **38**(1) 03-10